Synthesis, Characterization, Biophysical and Chemical Properties of Benzo[b]thiophene Derivatives and its Metal Complexes

T. M. Dhanya[1], K.J. Rajimon[2], Jibin. K. Varughese[3], K. G. Raghu[4], G. Anjali Krishna[5], Sachin Philip[1], Saumya. S. Pillai[6], P. A. Rineesh[7], Priya Breitener[8] and P. V. Mohanan[1,*]

[1]Department of Applied Chemistry, Cochin University of Science and Technology, Kochi 22, Kerala, India, Email: mohan@cusat.ac.in

[2]Department of Chemistry, St. Berchmans College, Changanacherry, Kerala, India, Email:rajimonkalambukattu@gmail.com

[3]Jr. HSST Chemistry, KMHSS Kuttoor, North Malappuram, India, Email: jibinkchem@gmail.com

[4]Agro-Processing and Technology Division, CSIR-National Institute for Interdisciplinary Science and Technology, Thiruvananthapuram, *Kerala, India, Email:raghukgopal@niist.res.in*

[5]Department of Science and Humanities, Mar Baselios Institute of Technology and Science, Nellimattom, Kothamangalam, Kerala, India, Email:anjalikrishna@mbits.ac.in

[6]Post Graduate and Research Department of Chemistry, NSS Hindu College, Changanacherry, Kerala, India, Email: saumyaspillai@gmail.com

[7]School of Chemical Sciences, Mahatma Gandhi University, Kottayam, Kerala, India, Email:rineeshasokan2011@gmail.com

[8]Fatima College of Health Science, General Requirement Department, Abu Dhabi, United Arab Emirates, Email:priya.breitener@actvet.gov.ae

Scheme S1. The process involved in the synthesis of the Schiff base ligand BA.

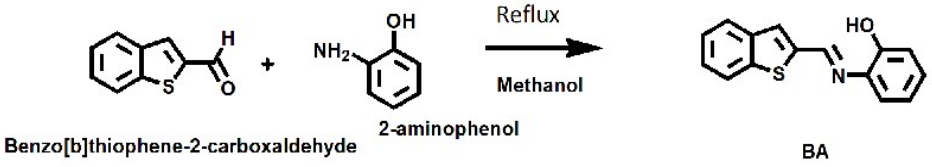

Benzo[b]thiophene-2-carboxaldehyde 2-aminophenol BA

Scheme S2. The synthetic route involved in the formation of the Schiff base ligand BMP.

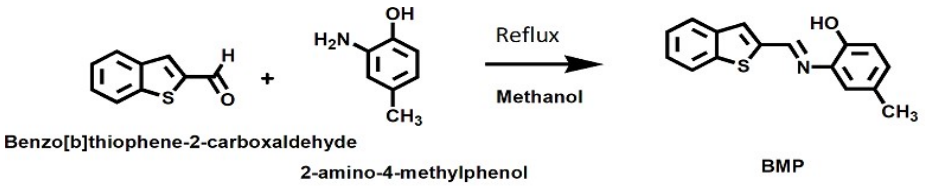

Benzo[b]thiophene-2-carboxaldehyde

2-amino-4-methylphenol

BMP

Scheme S3. The synthetic route involved in the formation of the Schiff base ligand BNP.

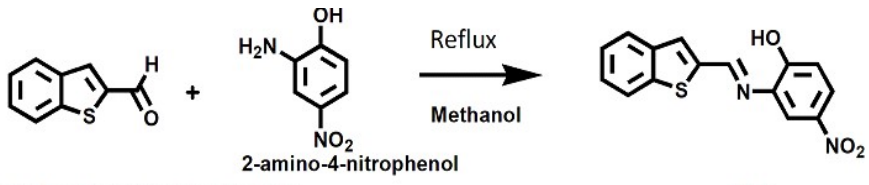

2-amino-4-nitrophenol

Benzo[b]thiophene-2-carboxaldehyde

BNP

Scheme S4. The synthetic route involved in the formation of the Schiff base ligand 4BNP.

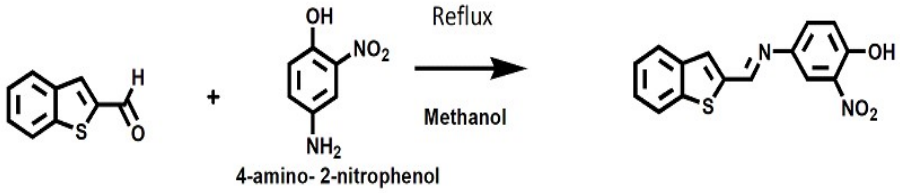

4-amino- 2-nitrophenol

Benzo[b]thiophene-2-carboxaldehyde

4BNP

Scheme S5. The scheme shows the synthesis of Ni(II) and Mn(II) complexes derived from the benzo[b]thiophene Schiff base ligand BA.

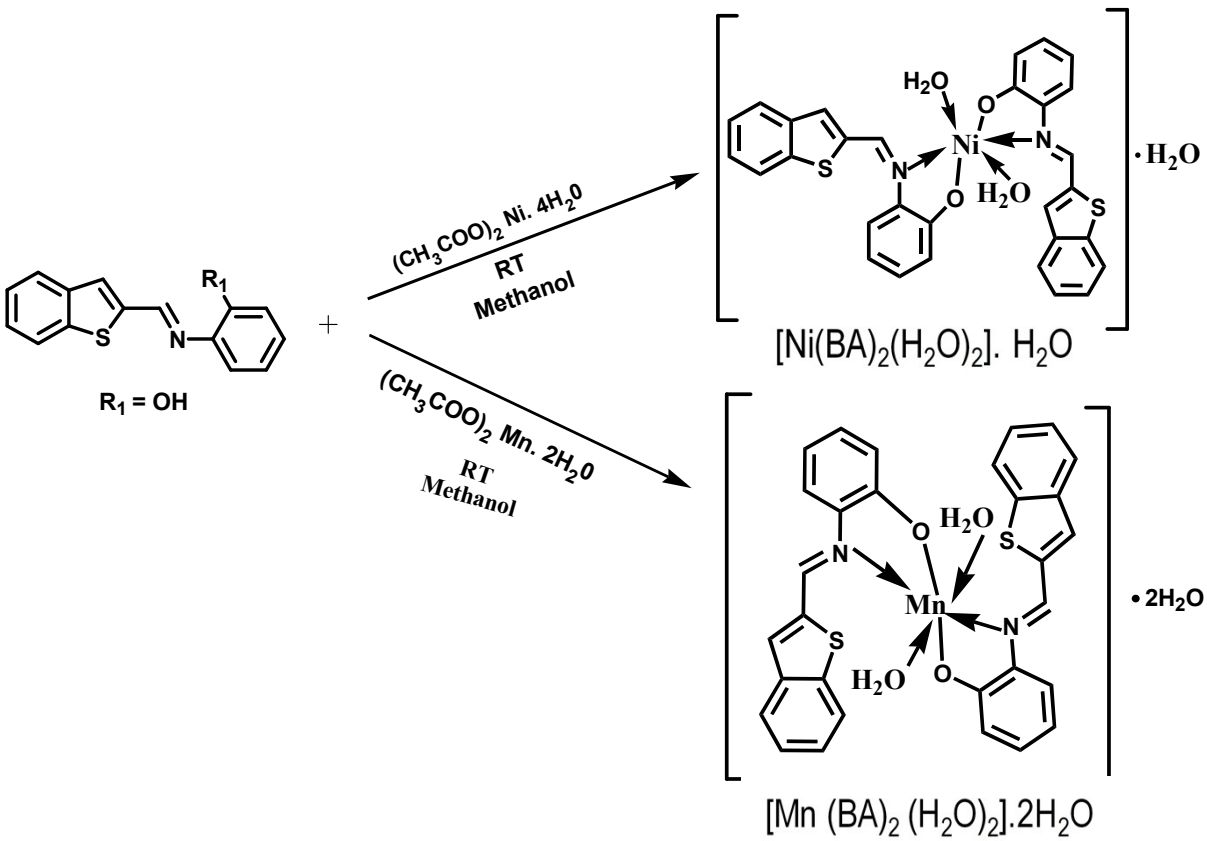

Scheme S6. The scheme shows the synthesis of Ni(II) and Mn(II) complexes derived from the benzo[b]thiophene Schiff base ligand BMP.

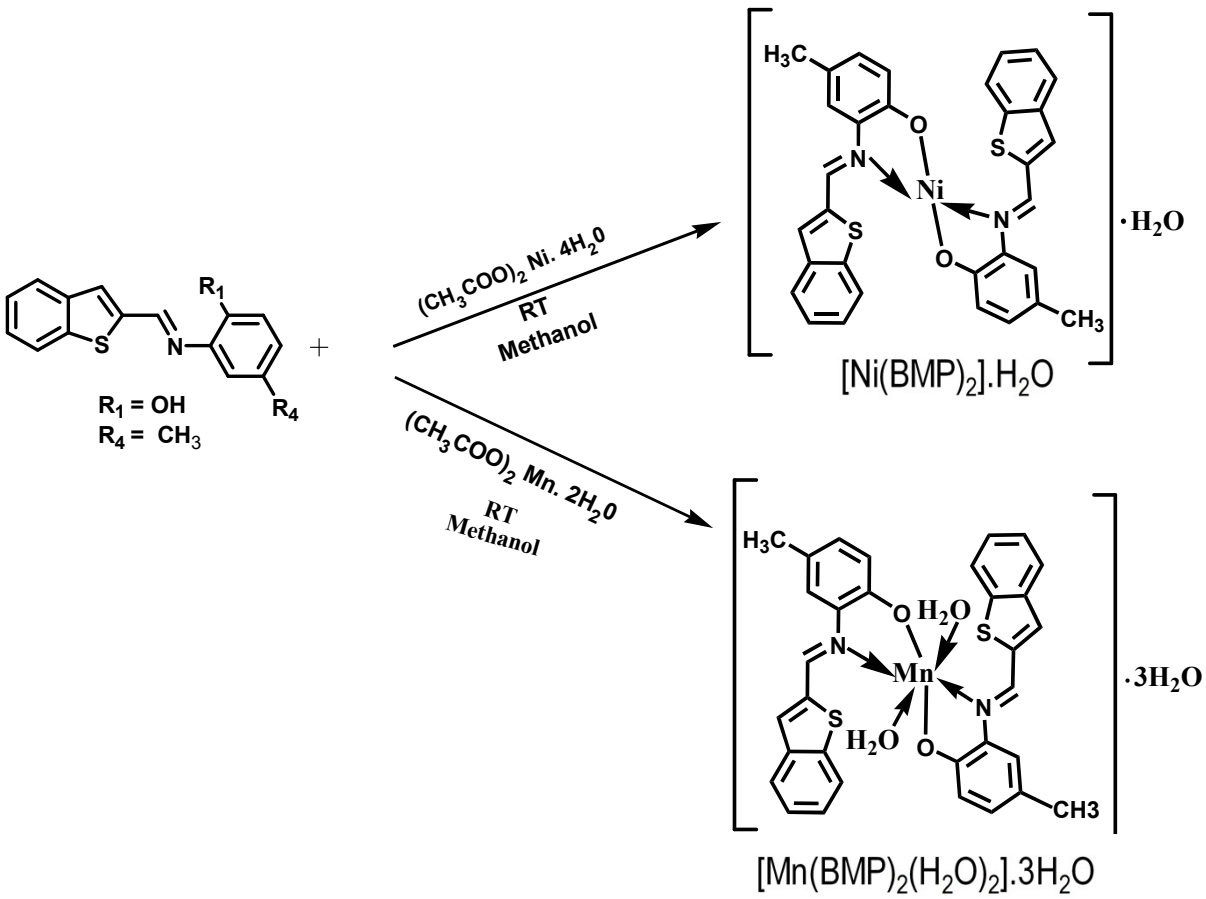

Scheme S7. The scheme shows the synthesis of Ni(II) and Mn(II) complexes derived from the benzo[b]thiophene Schiff base ligand BNP.

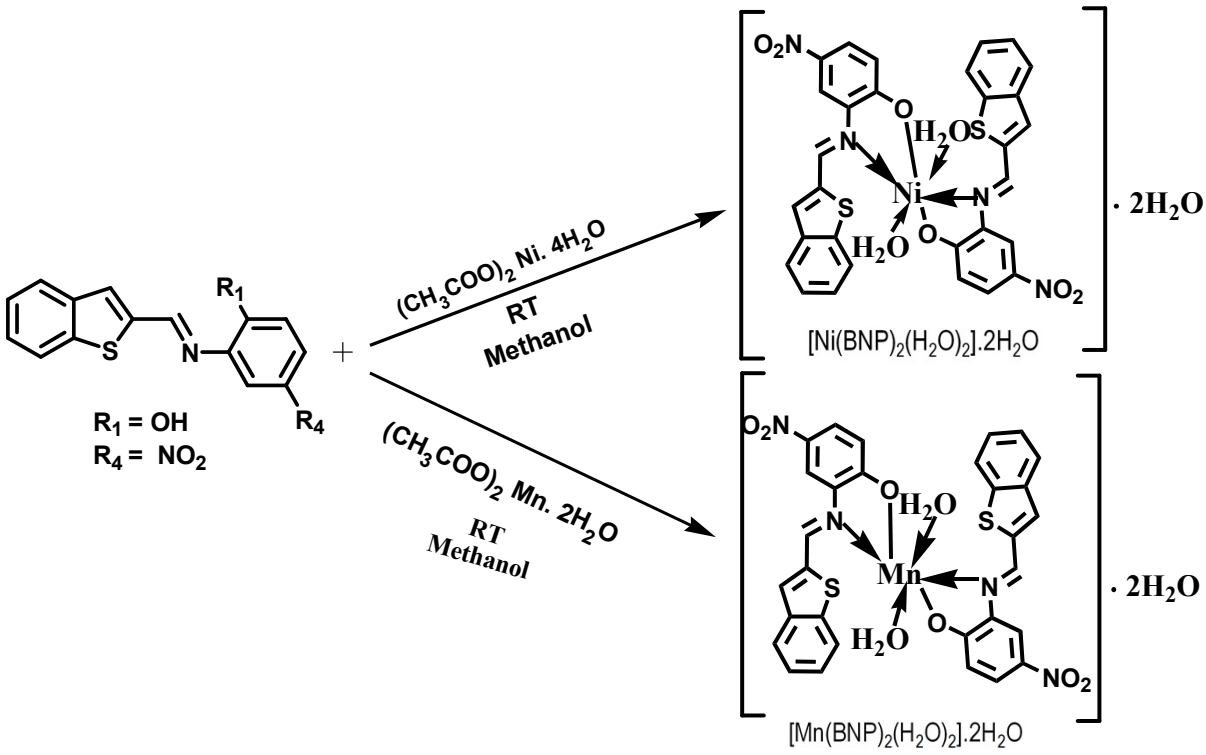

Scheme S8. The scheme shows the synthesis of Ni(II) and Mn(II) complexes derived from the benzo[b]thiophene Schiff base ligand 4BNP.

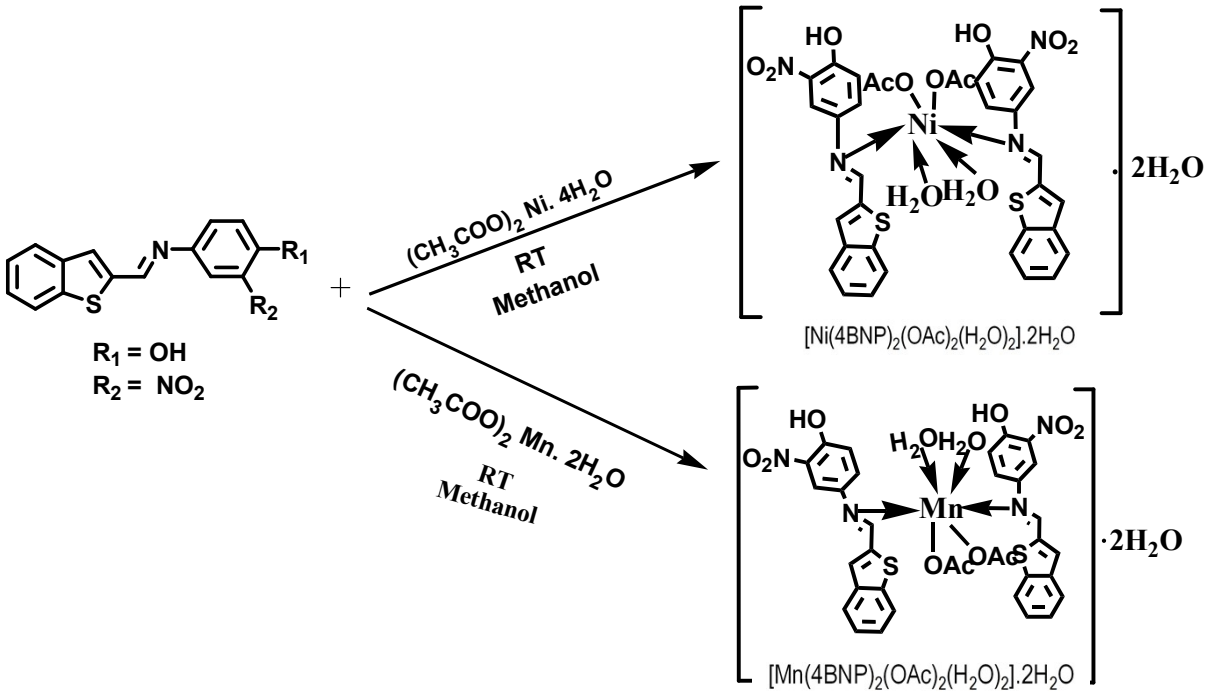

Fig. S1. The UV-visible absorption spectra of synthesized ligands BA and BMP indicating the characteristic π→π* and n → π* electronic transitions.

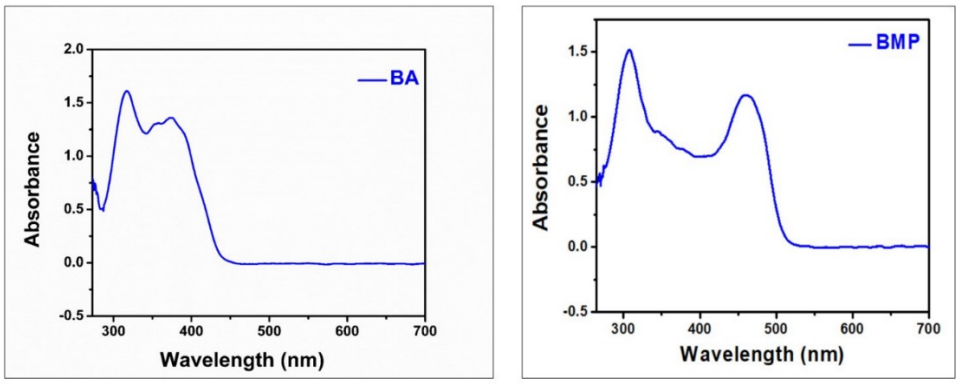

Fig. S2. The UV-visible absorption spectra of synthesized ligands BNP and 4BNP indicating the characteristic π→π* and n → π* electronic transitions.

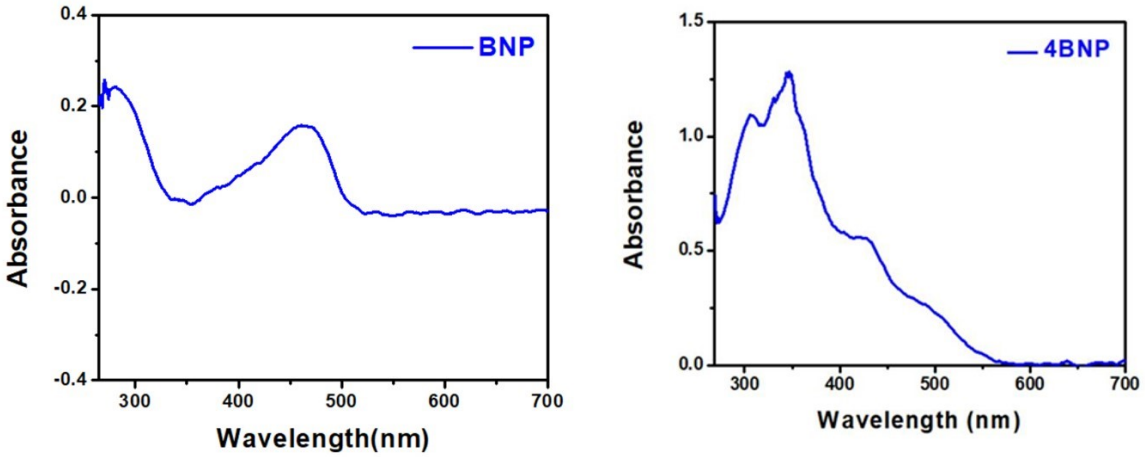

Fig. S3. Mass Spectrum of BA.

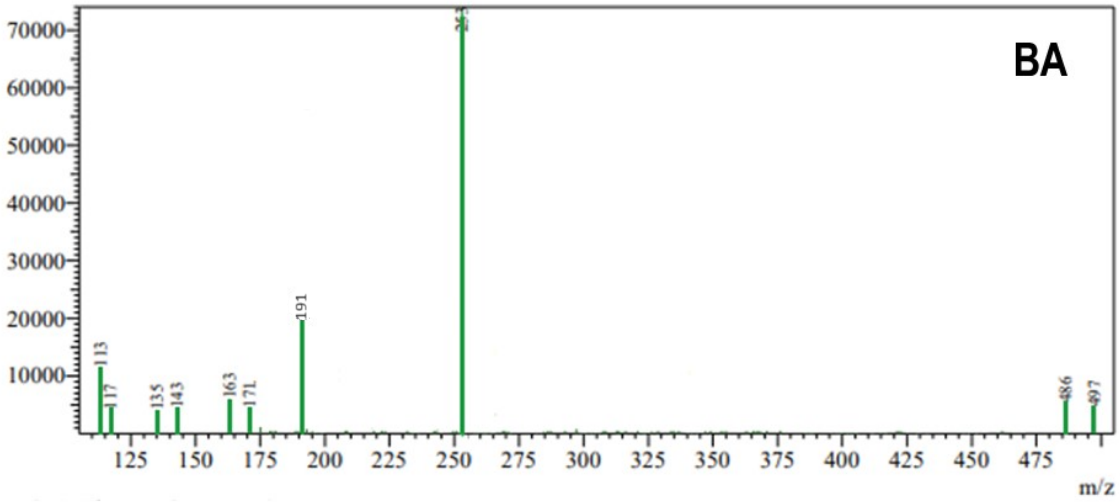

Fig. S4. Mass Spectrum of BMP.

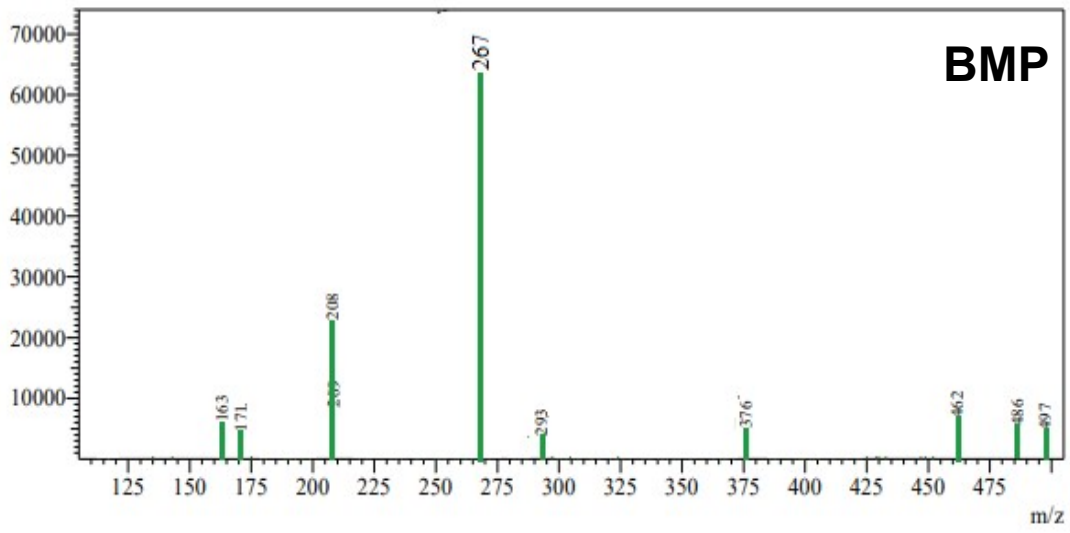

Fig. S5. Mass Spectrum of BNP.

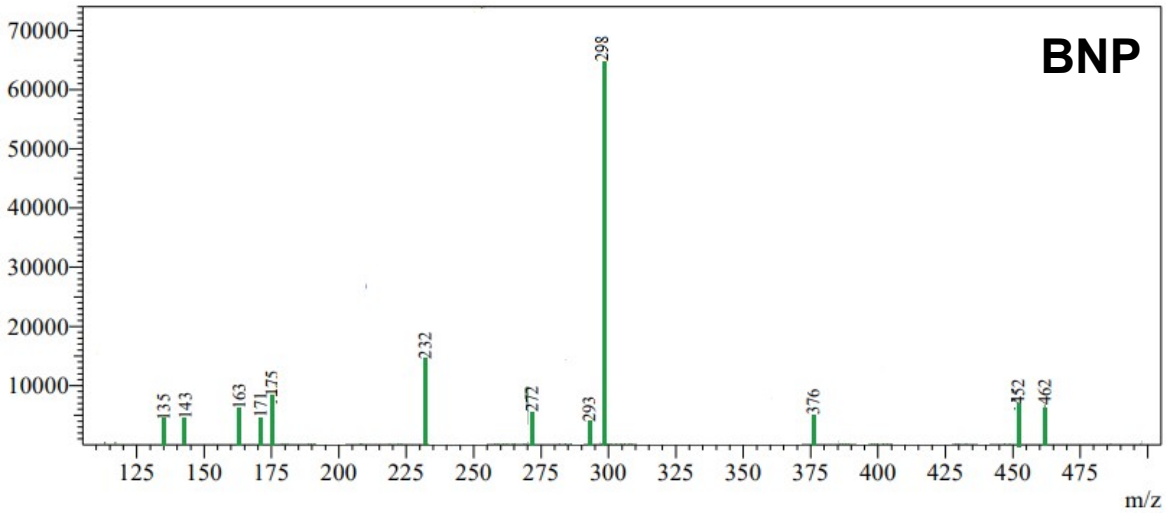

Fig. S6. Mass Spectrum of 4BNP.

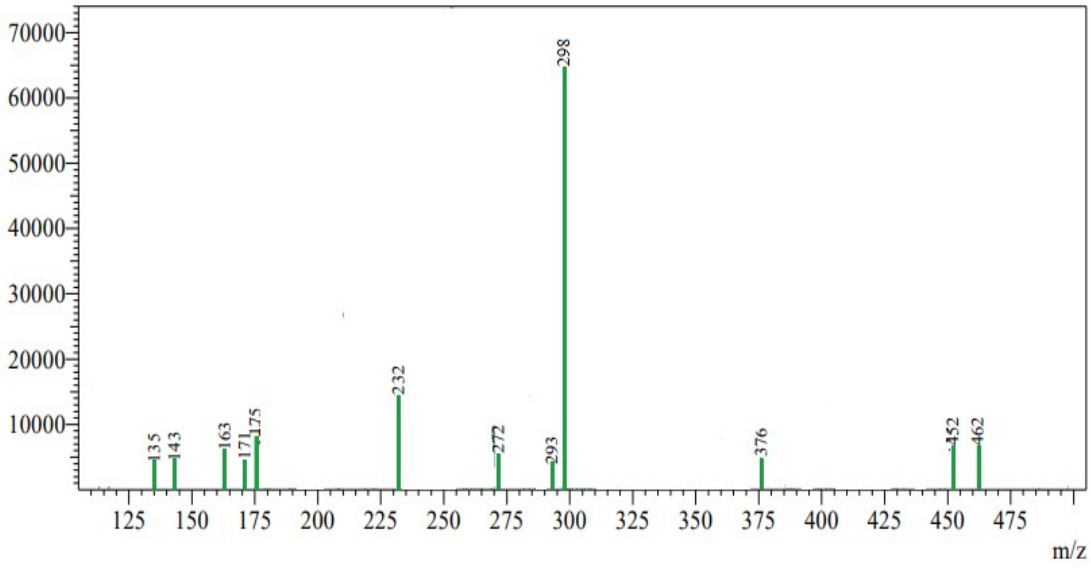

Fig. S7.[1]H NMR spectrum of BA.

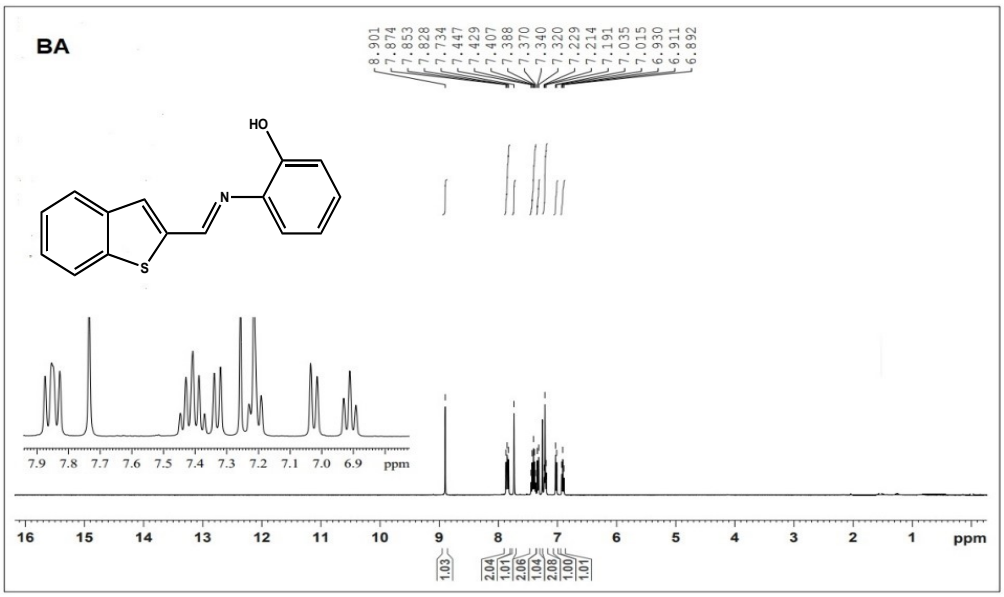

Fig. S8.[1]H NMR spectrum of BMP.

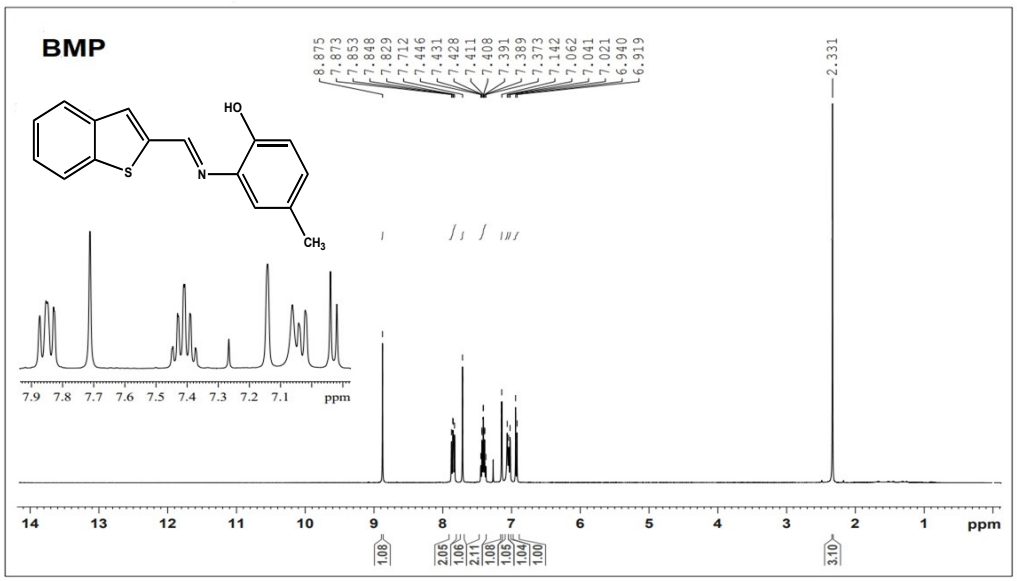

Fig. S9.[1]H NMR spectrum of BNP.

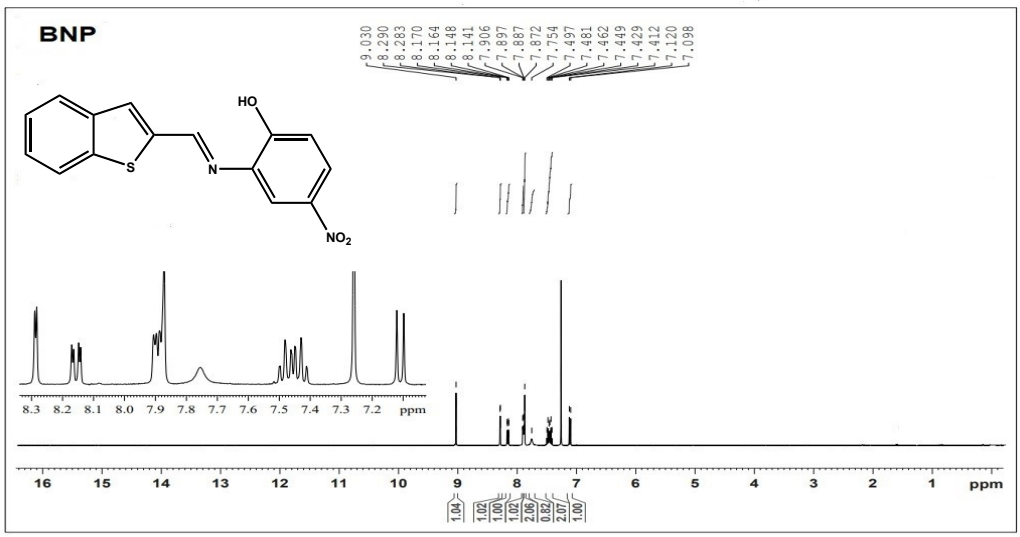

Fig. S10.[1]H NMR spectrum of 4BNP.

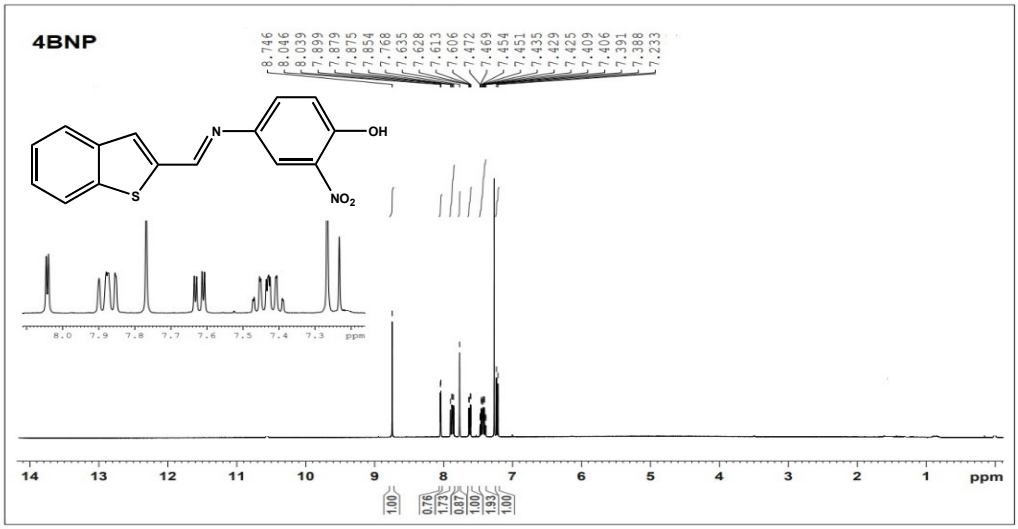

Fig. S11. ^{13}C NMR Spectrum of BA.

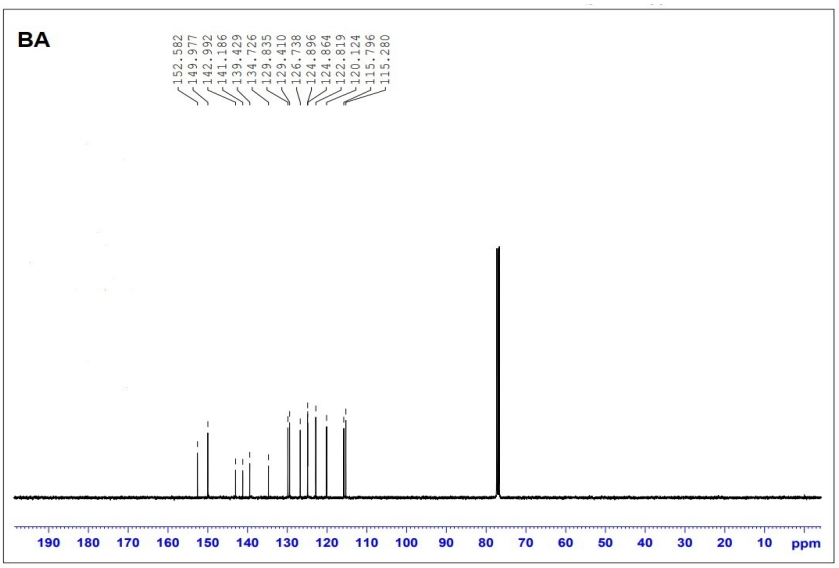

Fig. S12. ^{13}C NMR Spectrum of BMP.

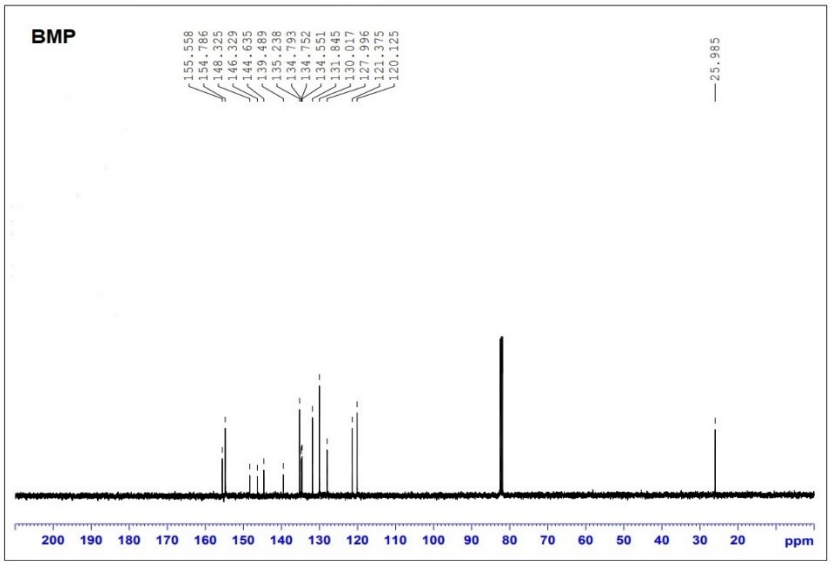

Fig. S13. ^{13}C NMR Spectrum of BNP.

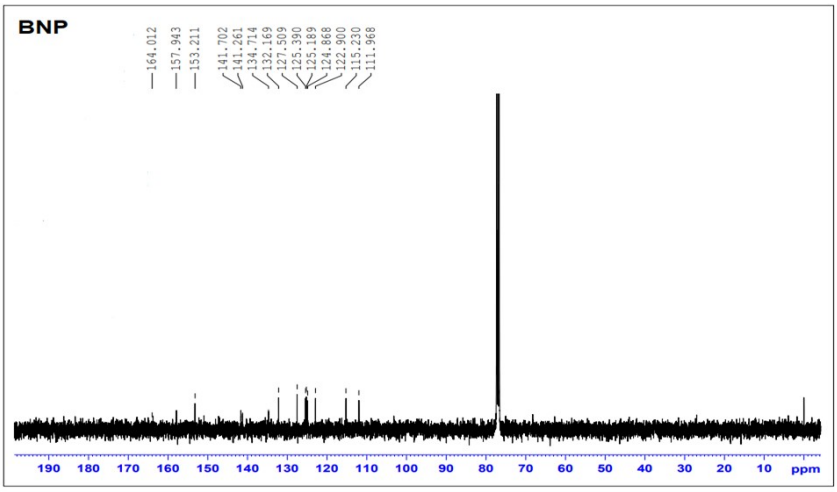

Fig.S14. ^{13}C NMR Spectrum of 4BNP.

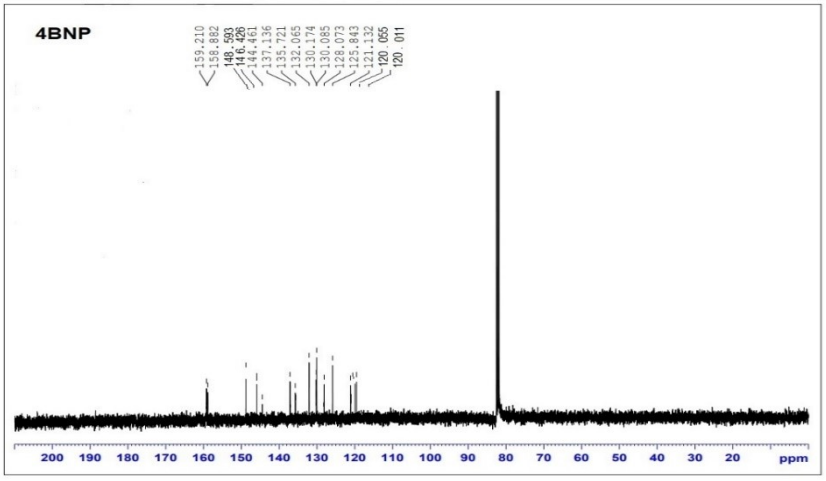

Fig. S15. The UV-visible absorption spectra of synthesized ligand incorporated metal complex BAN and BMPN.

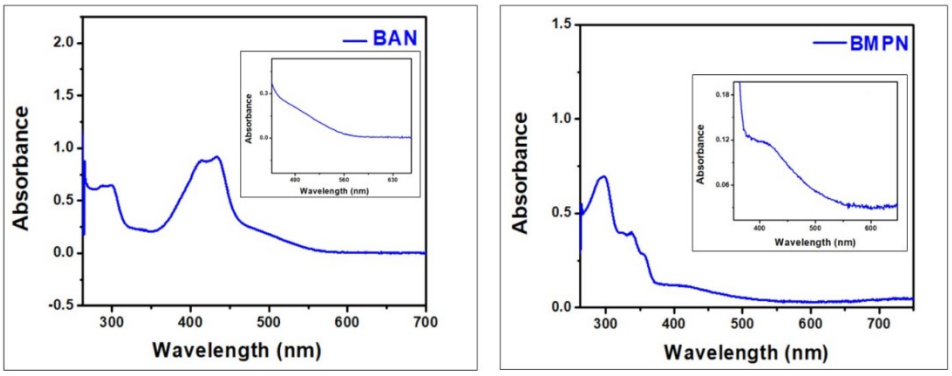

Fig. S16. The UV-visible absorption spectra of synthesized ligand incorporated metal complex BNPN and 4BNPN.

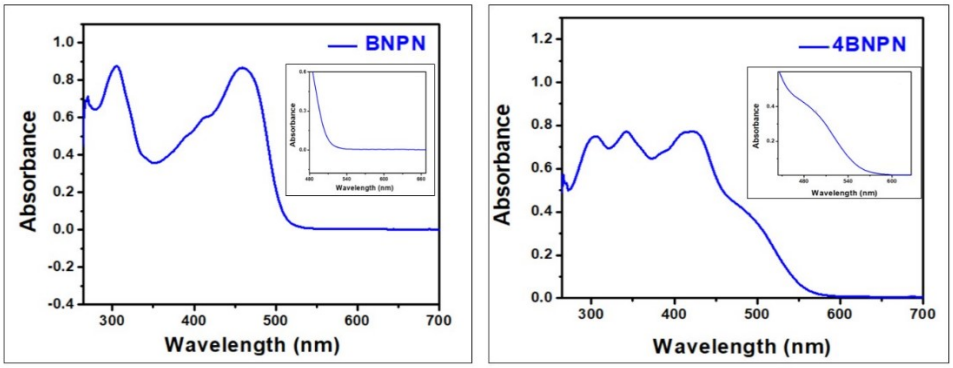

Fig. S17. The UV-visible absorption spectra of synthesized ligand incorporated metal complex BAM and BMPM.

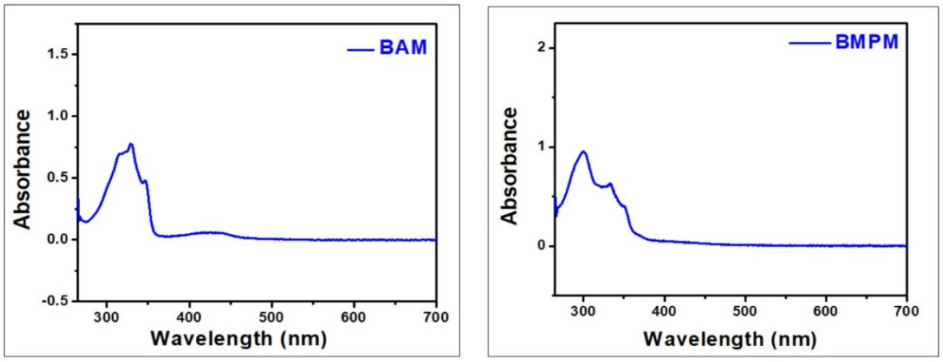

Fig. S18. The UV-visible absorption spectra of synthesized ligand incorporated metal complex BNPM and 4BNPM.

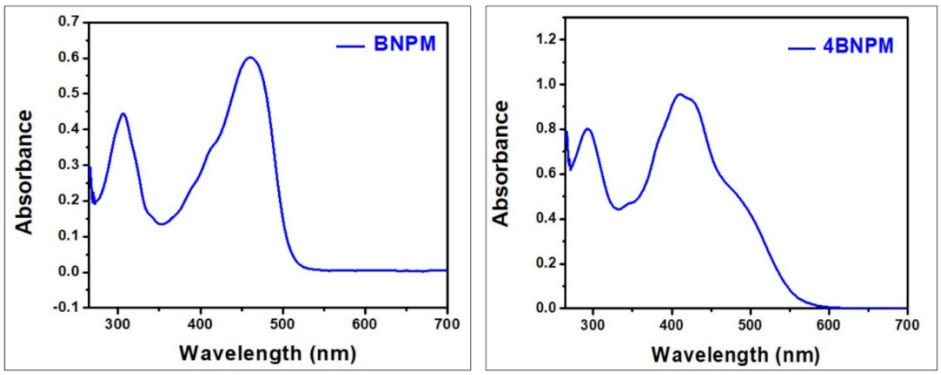

Fig.S19. IR spectra of the BA, BMP derived Ni(II) complex.

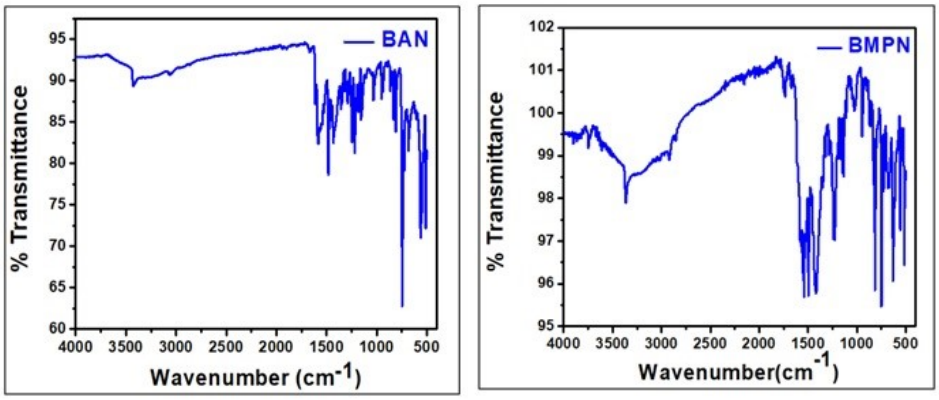

Fig.S20. IR spectra of the BNP, 4BNP derived Ni(II) complex.

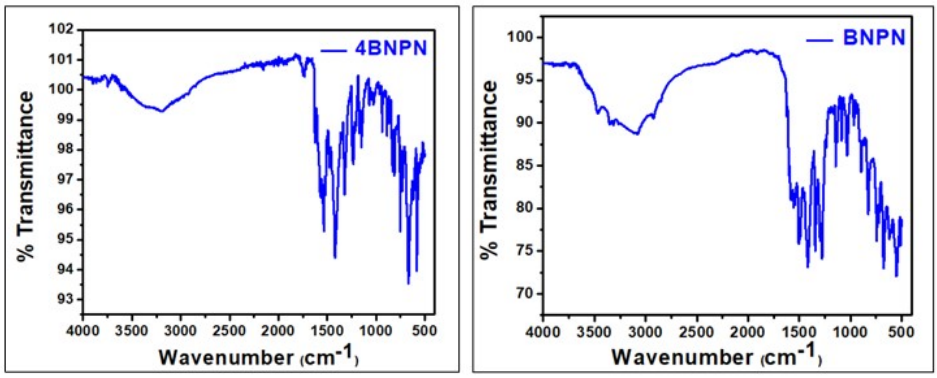

Fig.S21. IR spectra of the BA, BMP derived Mn(II) complex.

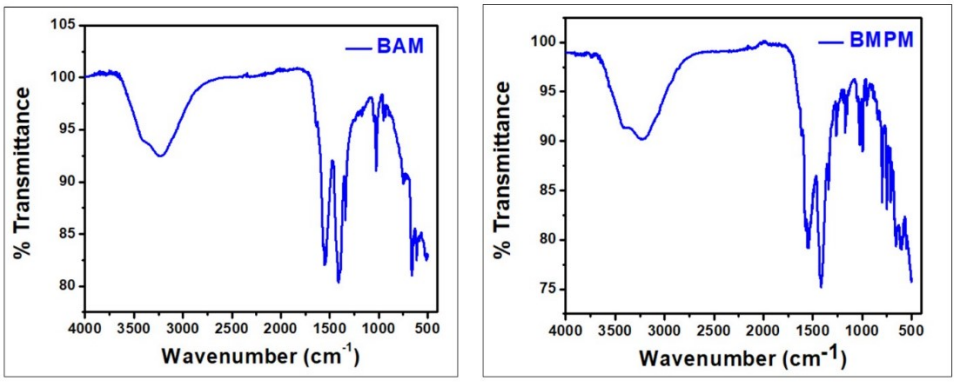

Fig.S22. IR spectra of the BA, BMP derived Mn(II) complex.

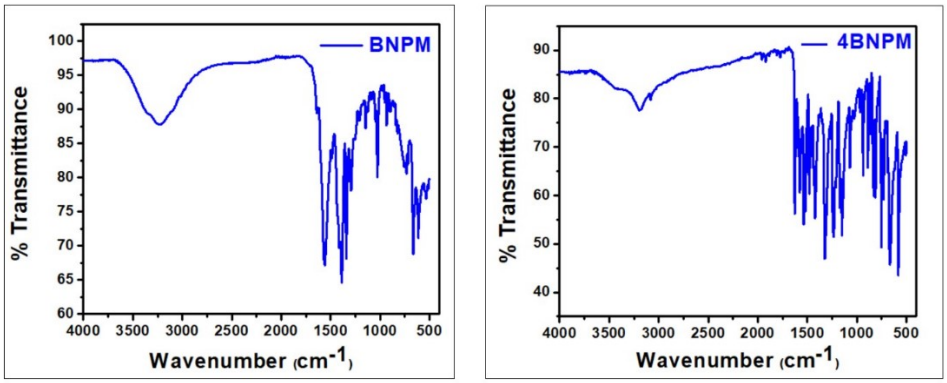

Fig.S23. TG-DTG graphs of Schiff base ligand BA, BMP incorporated metal complexes of Ni(II).

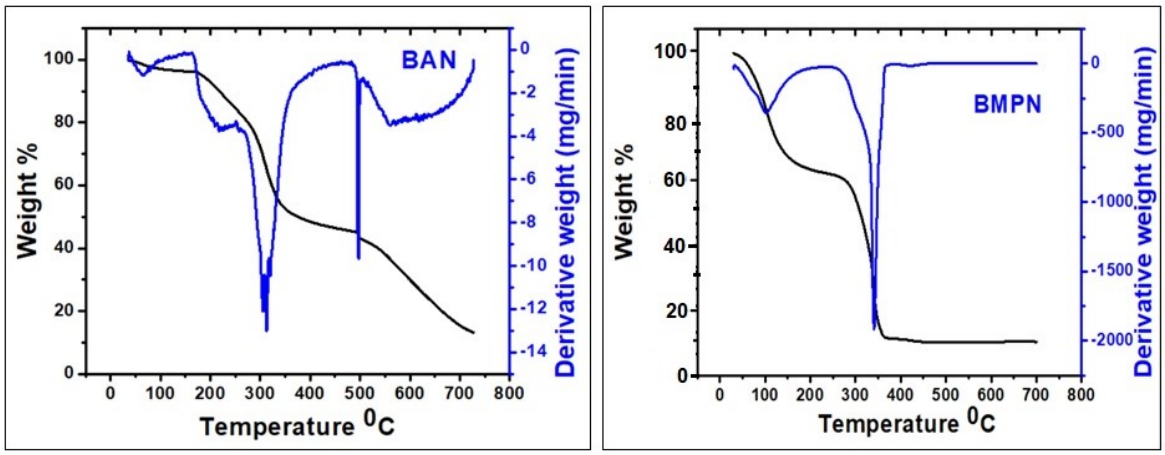

Fig.S24. TG-DTG graphs of Schiff base ligand BNP, 4BNP incorporated metal complexes of Ni(II).

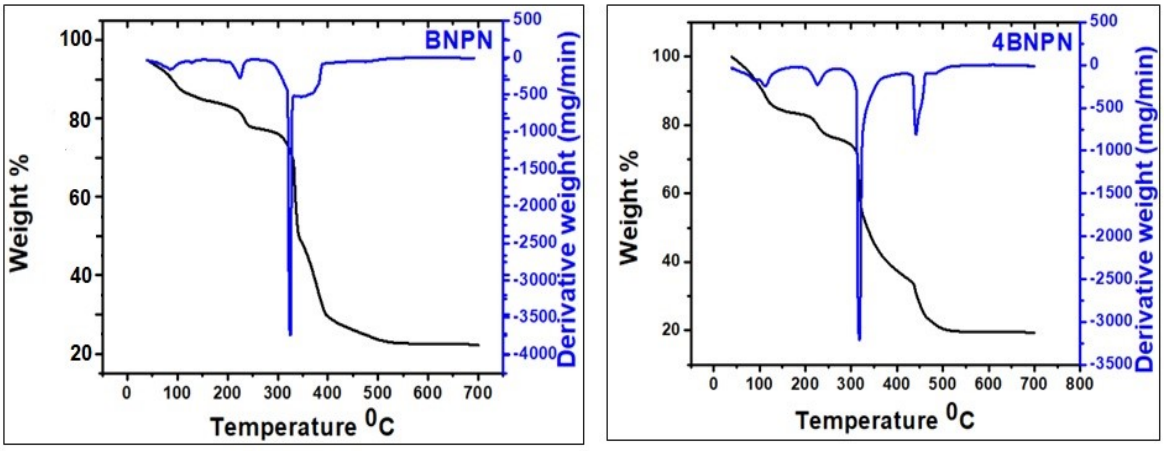

Fig.S25. TG-DTG graphs of Schiff base ligand BA, BMP incorporated metal complexes of Mn(II).

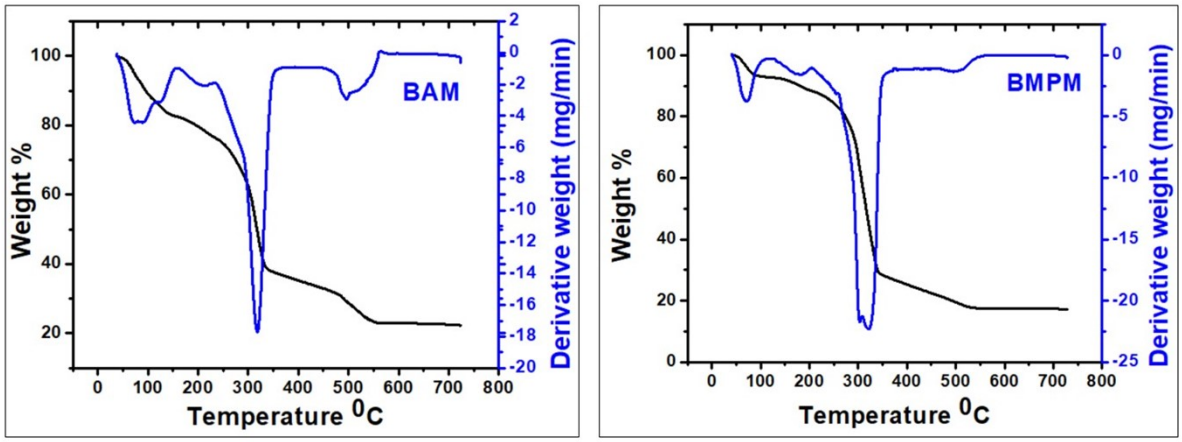

Fig.S26. TG-DTG graphs of Schiff base ligand BA, BMP incorporated metal complexes of Mn(II).

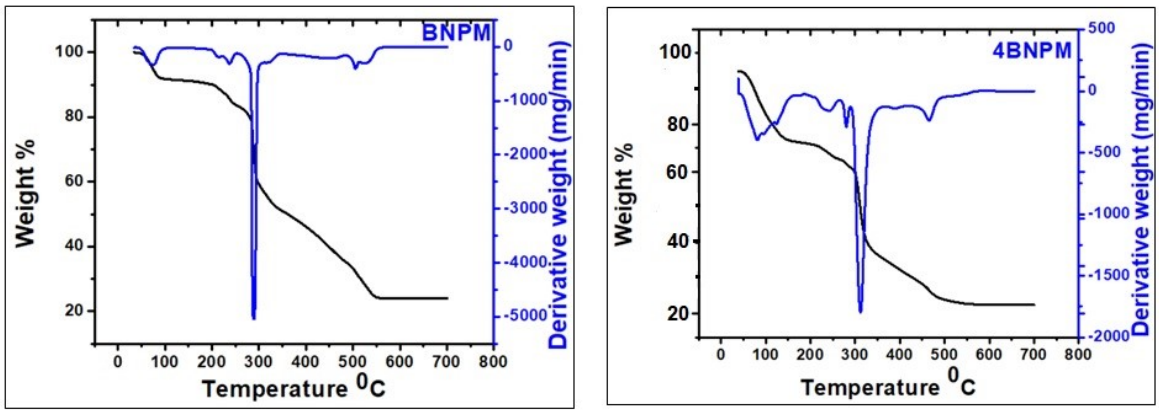

Fig. S27. Proposed structures of Mn(II) and Ni (II) complexes.

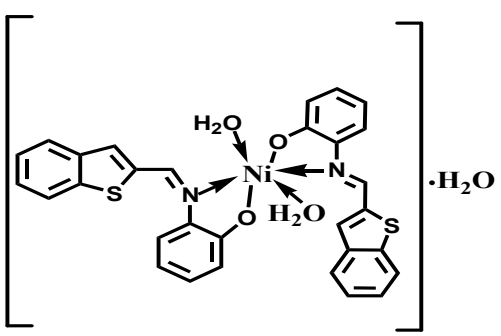

$[Ni(BA)_2(H_2O)_2].\ H_2O$

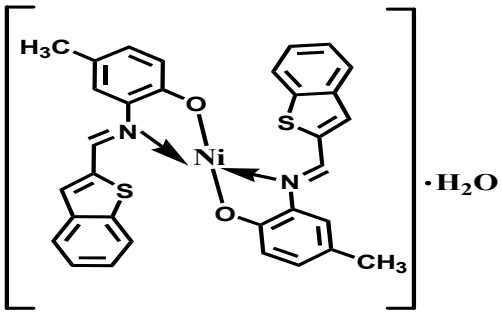

$[Ni(BMP)_2].H_2O$

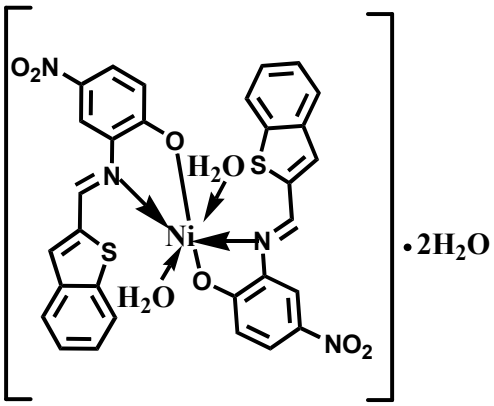

$[Ni(BNP)_2(H_2O)_2].2H_2O$

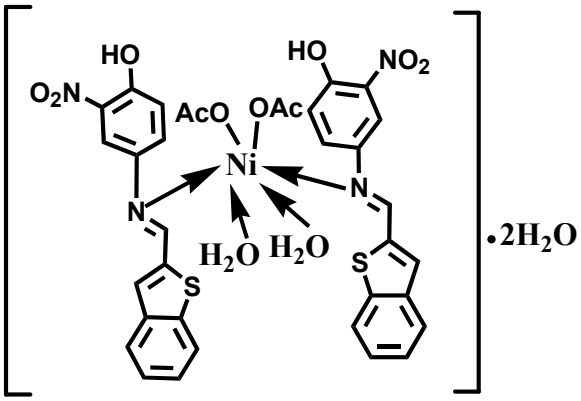

$[Ni(4BNP)_2(OAc)_2(H_2O)_2].2H_2O$

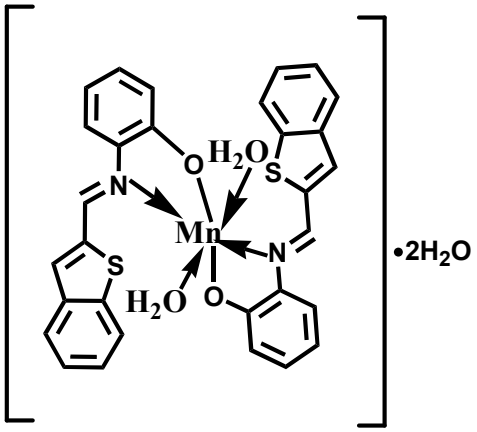

$[Mn\ (BA)_2\ (H_2O)_2].2H_2O$

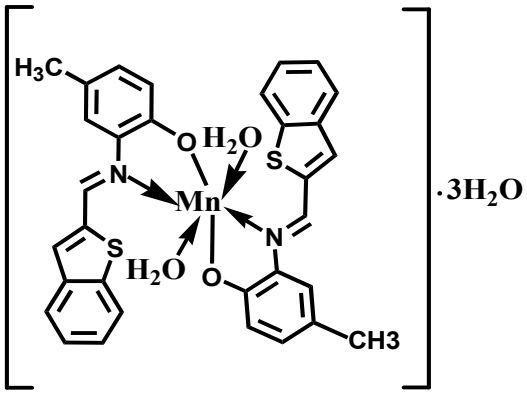

$[Mn(BMP)_2(H_2O)_2].3H_2O$

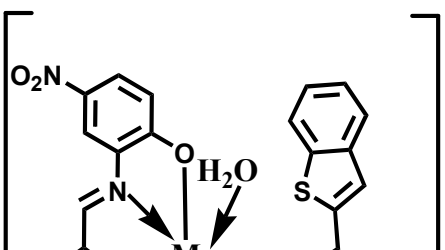

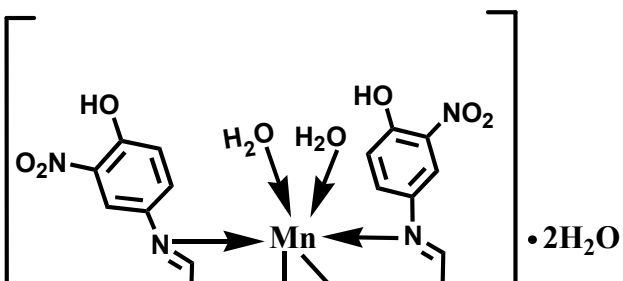

Fig. S28. The MM plot showing the α-amylase inhibition of the Schiff base ligand BA and their Ni(II), and Mn(II) complexes.

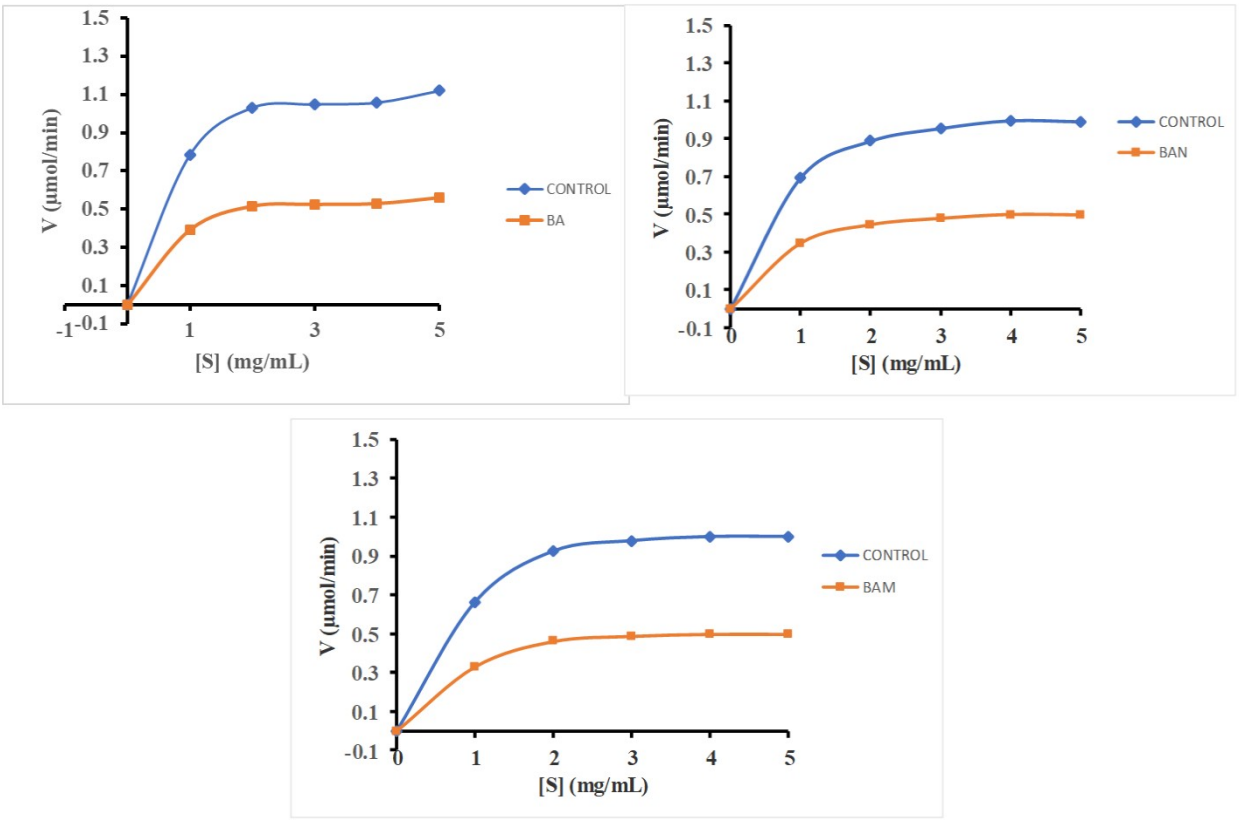

Fig. S29. The MM plot showing the α-amylase inhibition of the Schiff base ligand BMP and their Ni(II), and Mn(II) complexes.

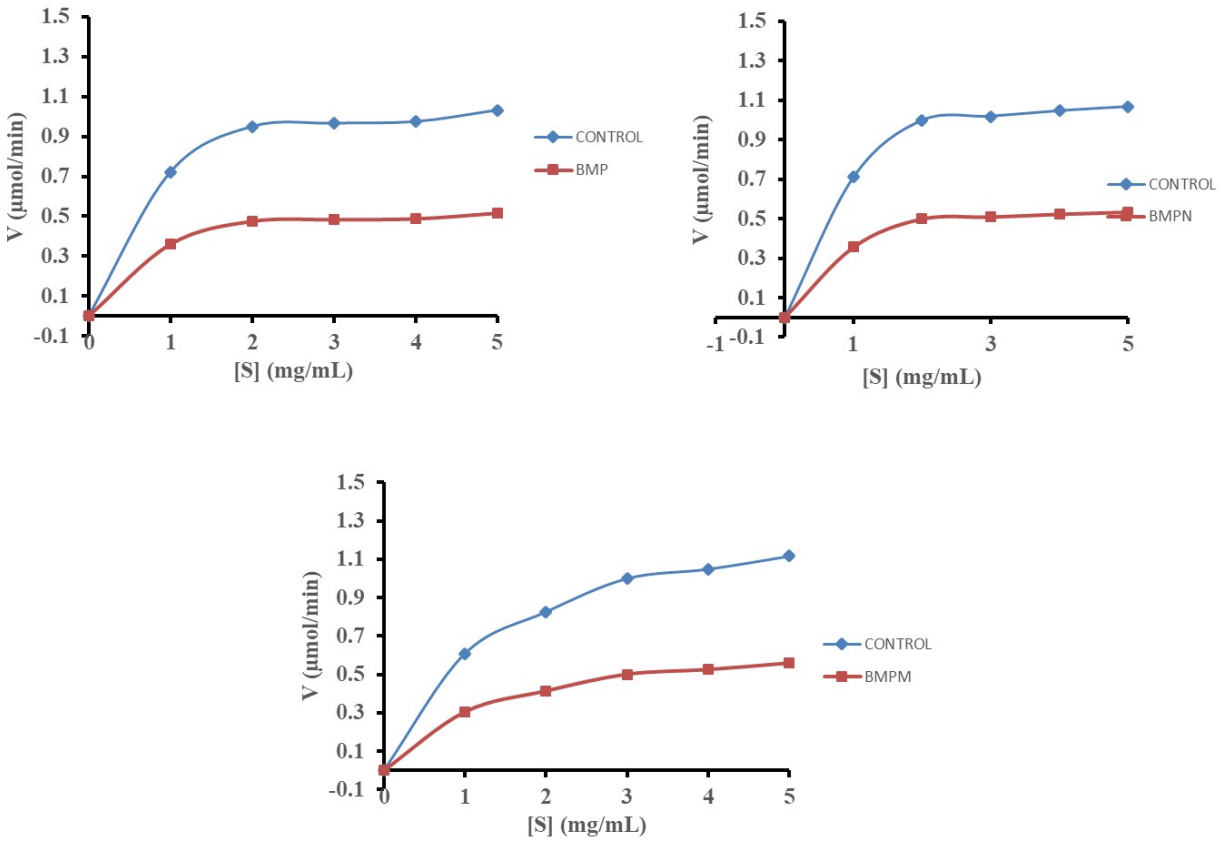

Fig. S30. The MM plot showing the α-amylase inhibition of the Schiff base ligand BNP and their Ni(II), and Mn(II) complexes.

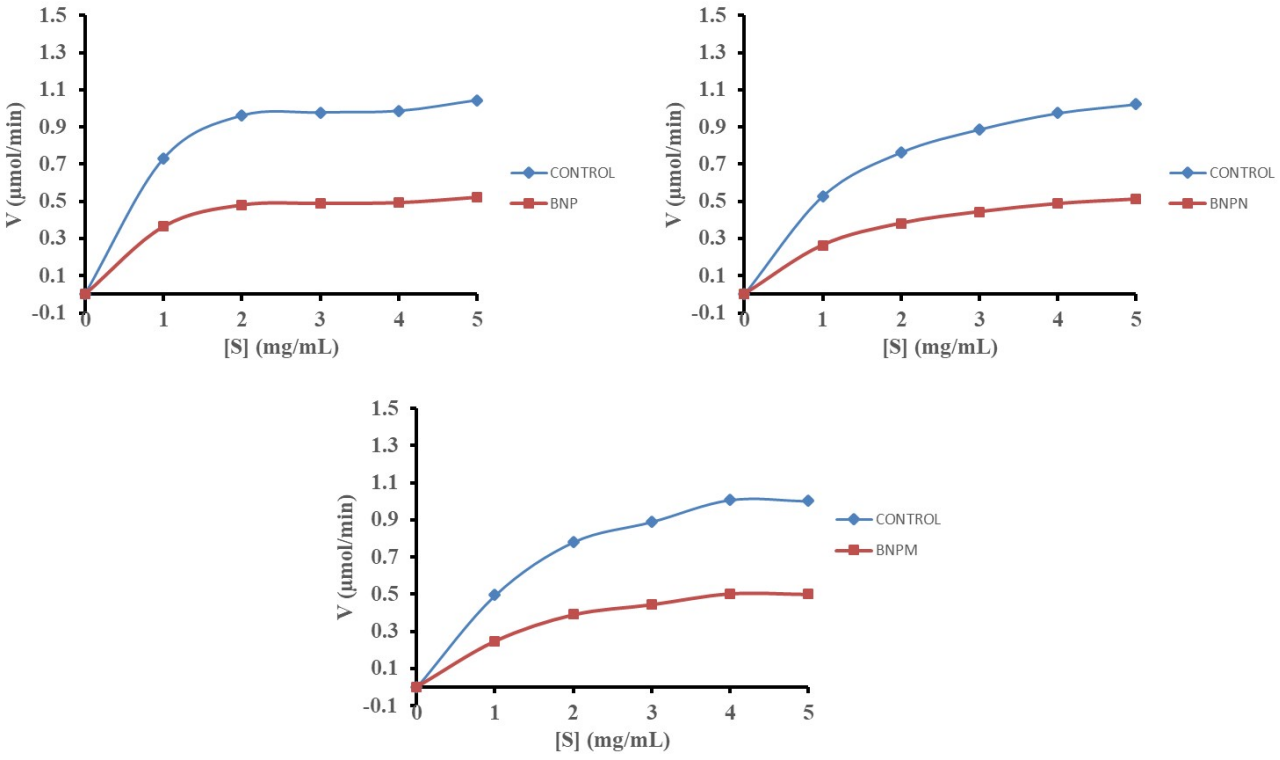

Fig. S31. The MM plot showing the α-amylase inhibition of the Schiff base ligand 4BNP and their Ni(II), and Mn(II) complexes.

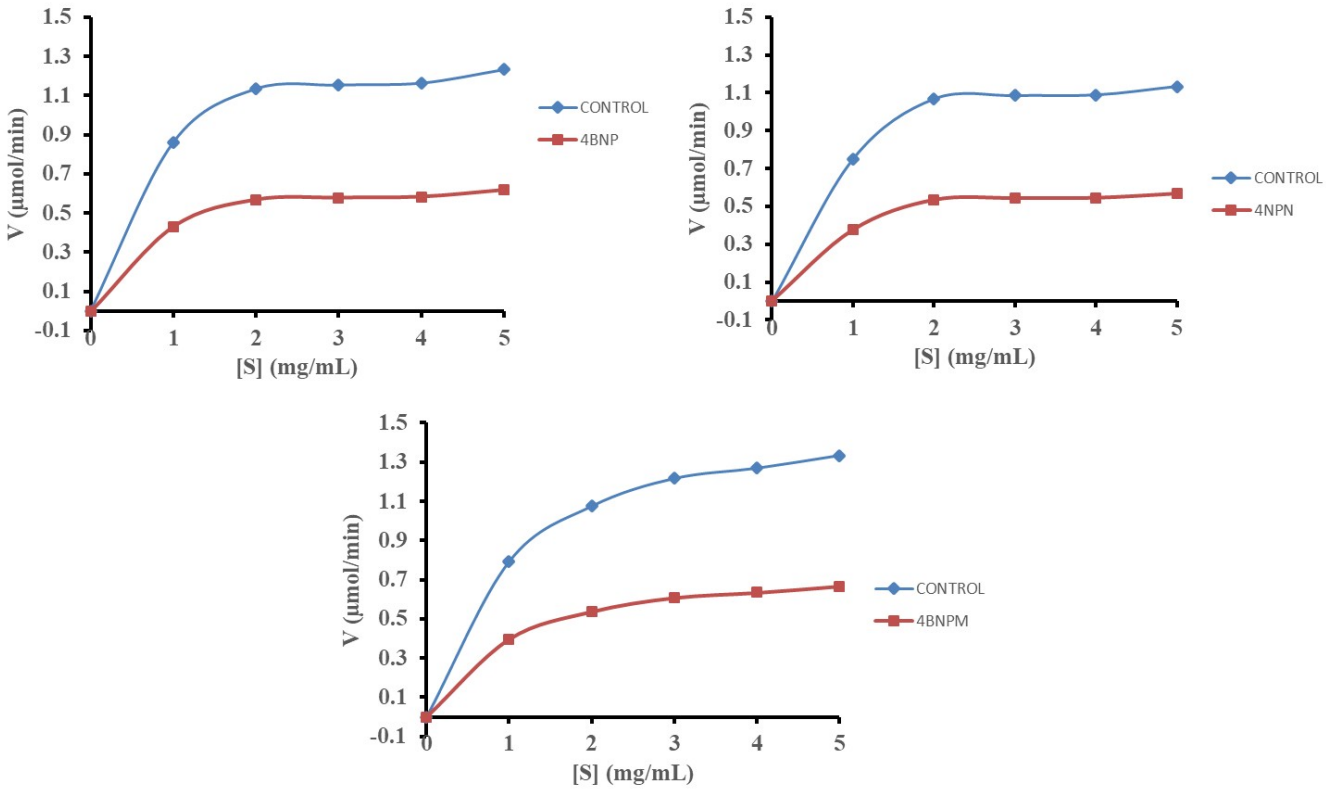

Fig. S32. The LB plot analysis showing the α-amylase inhibition of the Schiff base ligand BA and their Ni(II), and Mn(II) complexes.

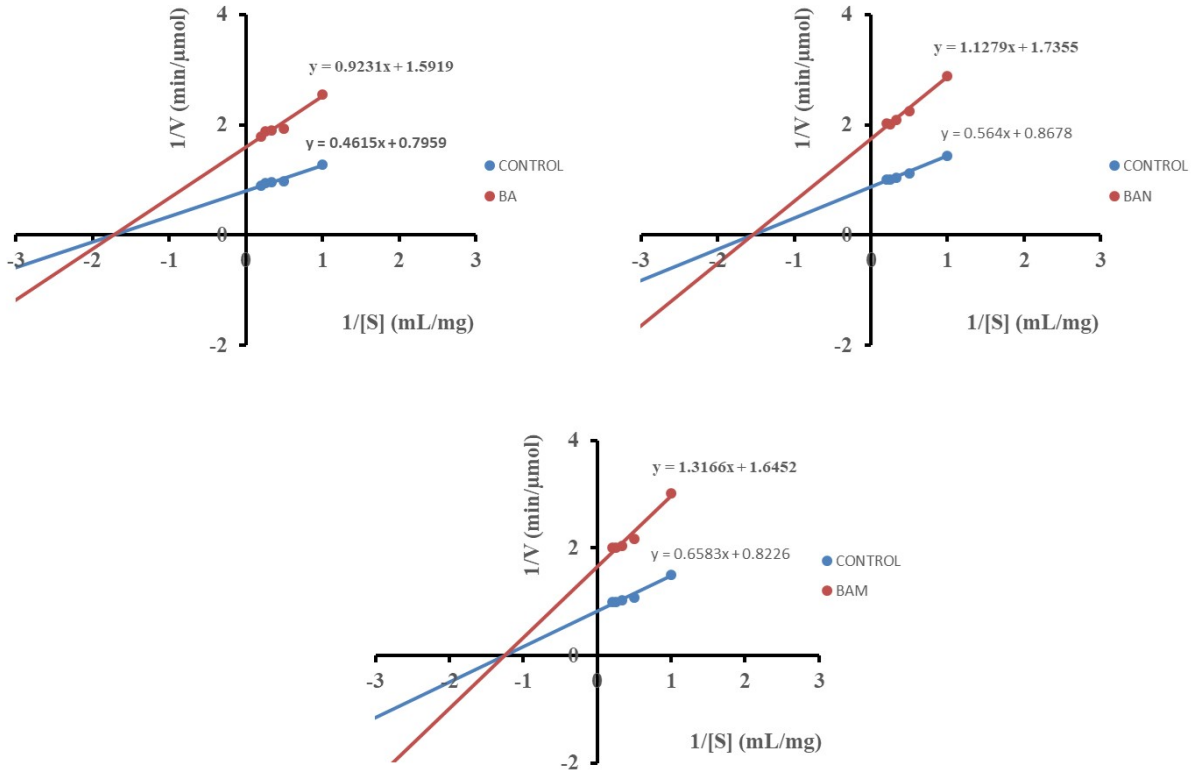

Fig. S33. The LB plot analysis showing the α-amylase inhibition of the Schiff base ligand BMP and their Ni(II), and Mn(II) complexes.

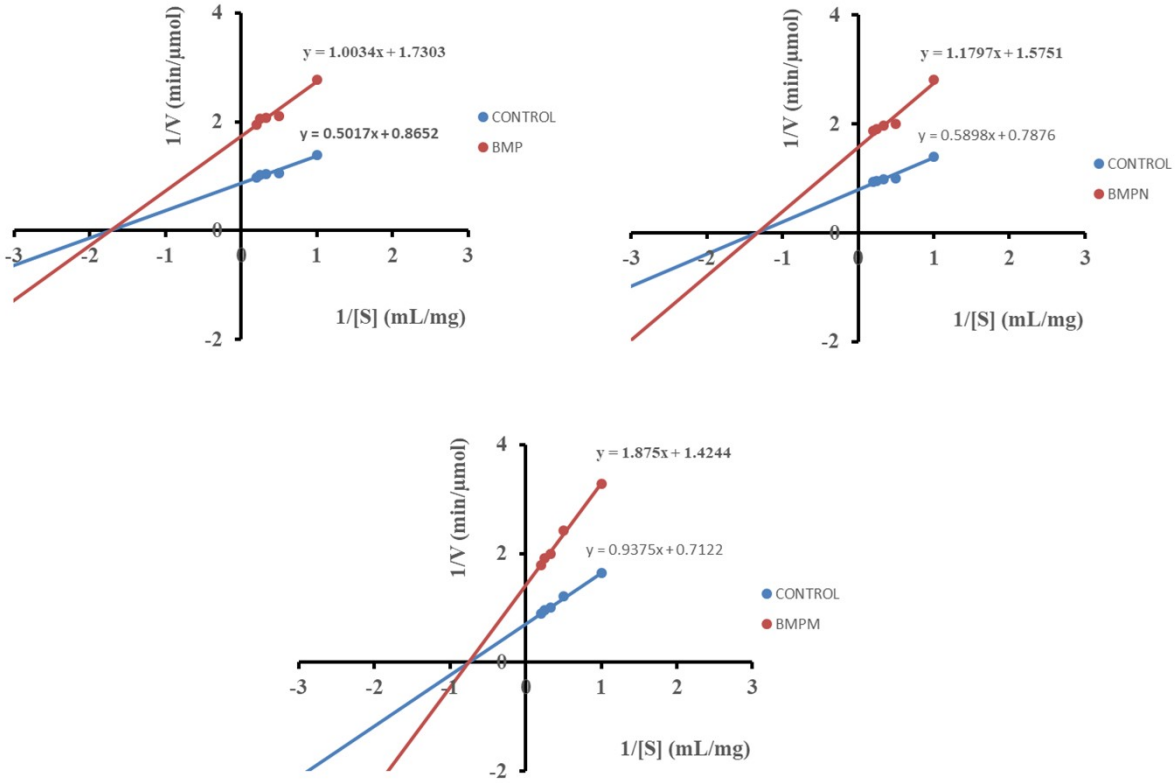

Fig. S34. The LB plot analysis showing the α-amylase inhibition of the Schiff base ligand BNP and their Ni(II), and Mn(II) complexes.

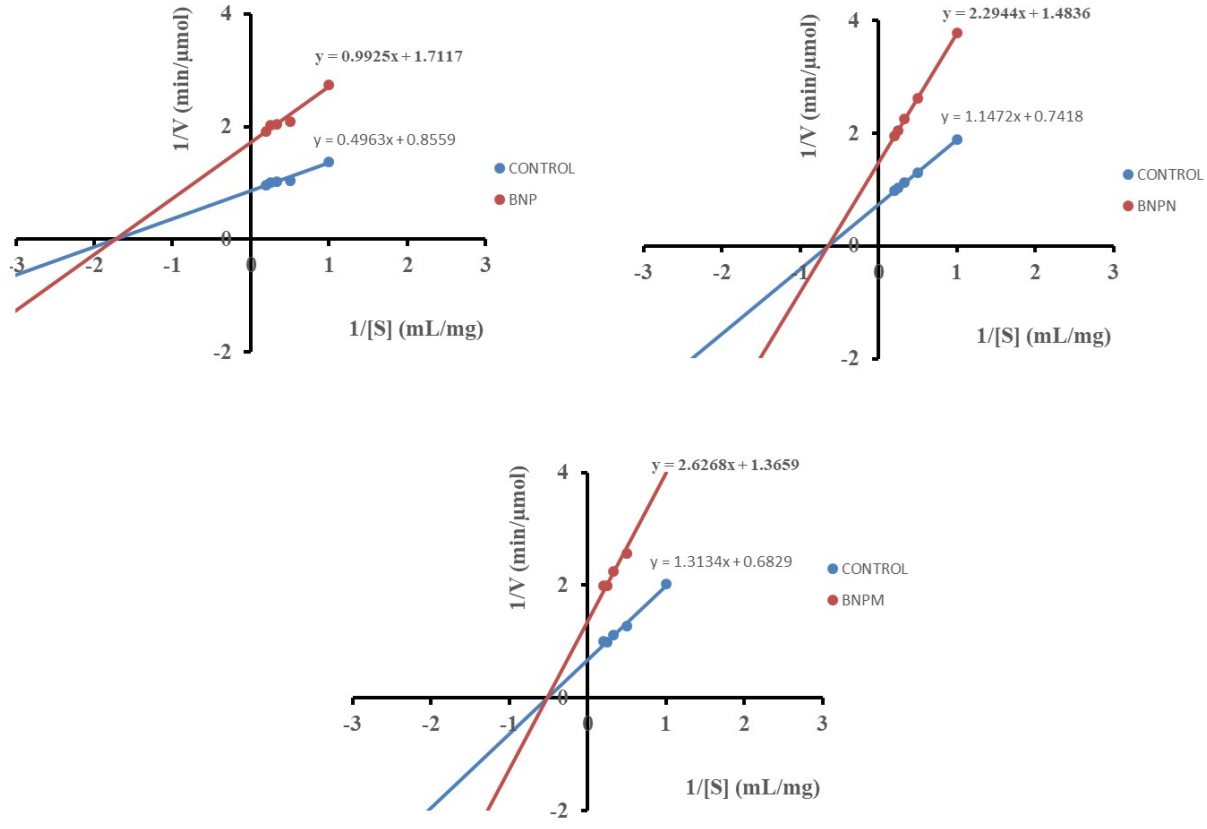

Fig. S35. The LB plot analysis showing the α-amylase inhibition of the Schiff base ligand 4BNP and their Ni(II), and Mn(II) complexes.

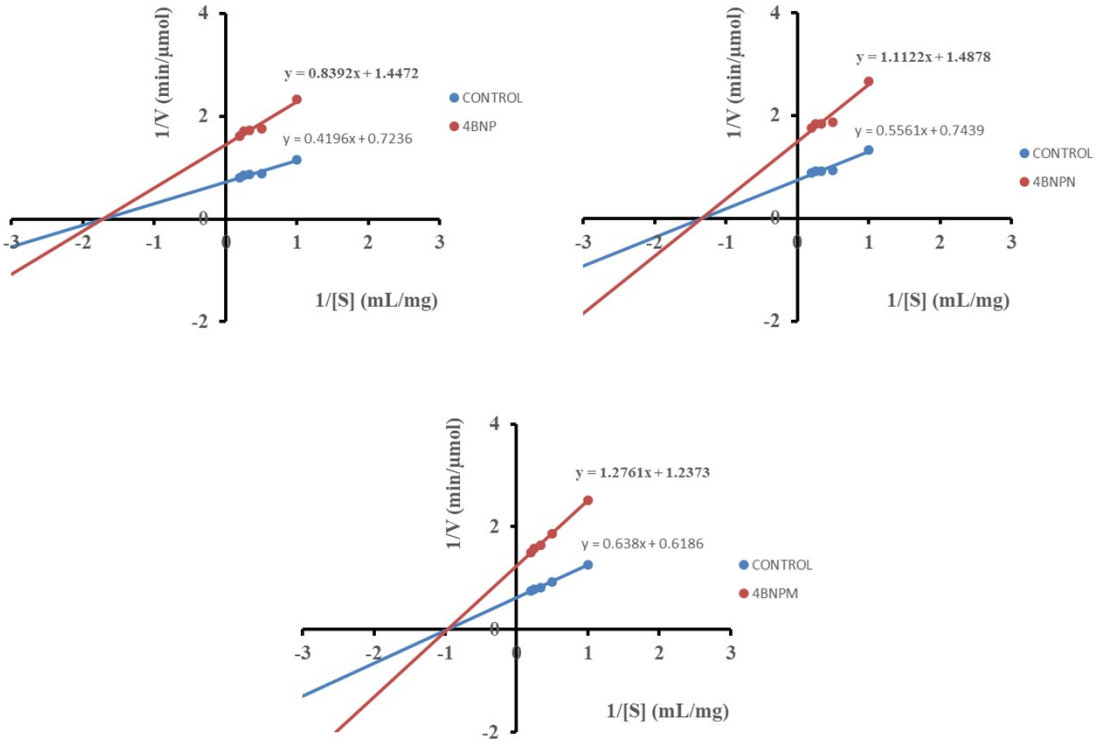

Fig. S36. The optimized structures of the benzo[b]thiophene Schiff base ligands BA, BMP, BNP and 4BNP.

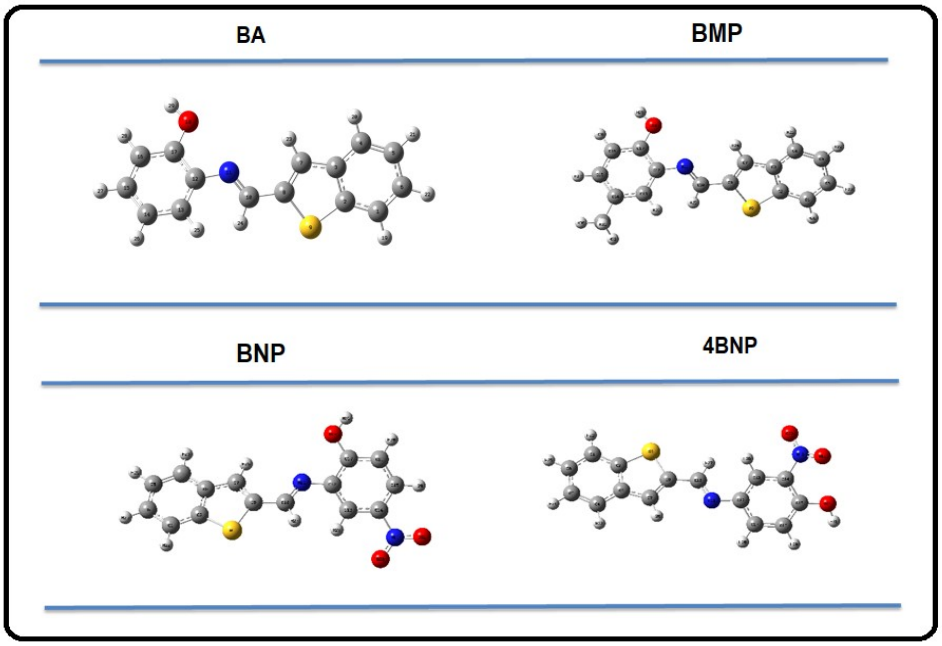

Fig. S37. The optimized structures of the Ni(II) and Mn(II) complexes derived from benzo[b]thiophene Schiff base ligands.

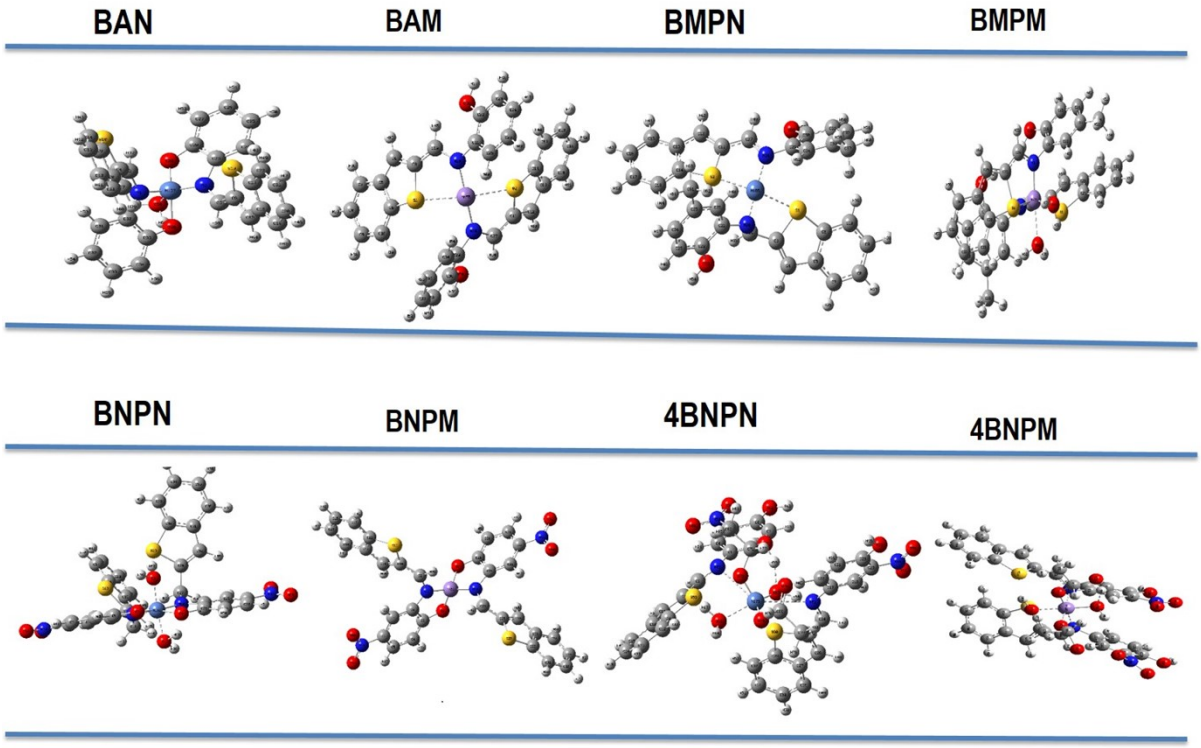

Table S1. The synthesis and compositional details of the ligand BA, BMP, BNP and 4BNP.

Compound	Empirical formula	Formula weight	mp °C	Color (yield %)	Calculated (found %)				
					C	H	N	O	S
BA	$C_{15}H_{11}NOS$	253.32	142	Yellow (86)	71.12 (71.15)	4.38 (4.42)	5.53 (5.55)	6.32 (6.33)	12.66 (12.69)
BMP	$C_{16}H_{13}NOS$	267.35	123	Light Yellow (84)	71.88 (71.89)	4.90 (4.93)	5.24 (5.27)	5.98 (5.99)	11.99 (12.01)
BNP	$C_{15}H_{10}N_2O_3S$	298.32	184	Dark Greenish (82)	60.39 (60.42)	3.38 (3.40)	9.39 (9.41)	16.09 (16.12)	10.75 (10.77)
4BNP	$C_{15}H_{10}N_2O_3S$	298.32	177	Yellow (80)	60.39 (60.42)	3.38 (3.40)	9.39 (9.42)	16.09 (16.12)	10.75 (10.79)

Table S2. The analytical data of the Ni(II) complexes derived from the Schiff base ligands.

Complex	Molecular Formula (M.F.)	Formula Weight	Color (Yield %)	Elemental Analysis Found (calc) % (calc)				% of Metal Found
				C	H	N	S	Ni
BAN $[Ni(BA)_2(H_2O)_2].H_2O$	$C_{30}H_{26}N_2NiO_5S_2$	616.06	Dark Brown (72)	58.36 (58.38)	4.24 (4.26)	4.54 (4.57)	10.39 (10.43)	9.51 (9.52)
BMPN $[Ni(BMP)_2].H_2O$	$C_{32}H_{26}N_2NiO_3S_2$	608.07	Yellow (80)	63.07 (63.10)	4.30 (4.31)	4.60 (4.62)	10.52 (10.55)	9.63 (9.62)
BNPN $[Ni(BNP)_2(H_2O)_2].2H_2O$	$C_{30}H_{26}N_4NiO_{10}S_2$	724.04	Yellow (78)	49.67 (49.71)	3.61 (3.64)	7.72 (7.71)	8.84 (8.86)	8.09 (8.13)
4BNPN $[Ni(4BNP)_2(OA_C)_2(H_2O)_2].2H_2O$	$C_{35}H_{37}N_4NiO_{14}S_2$	859.11	Orange (76)	48.85 (48.84)	4.33 (4.37)	6.51 (6.53)	7.45 (7.44)	6.82 (6.85)

Table S3. The analytical data of the Mn(II) complexes derived from the Schiff base ligands.

Complex	Molecular Formula (M.F.)	Formula Weight	Color (Yield %)	Elemental Analysis Found (calc) %				% of Metal Found (calc)
				C	H	N	S	Mn
BAM $[Mn(BA)_2(H_2O)_2].2H_2O$	$C_{30}H_{28}Mn\ N_2O_6S_2$	631.08	Yellow (74)	57.05 (57.07)	4.47 (4.48)	4.44 (4.48)	10.15 (10.14)	8.70 (8.74)
BMPM $[Mn(BMP)_2(H_2O)_2].3H_2O$	$C_{33}H_{37}Mn\ N_2O_7S_2$	692.14	Dark Yellow (82)	57.22 (57.26)	5.38 (5.39)	4.04 (4.02)	9.26 (9.29)	7.93 (7.97)
BNPM $[Mn(BNP)_2(H_2O)_2].2H_2O$	$C_{30}H_{26}Mn\ N_4O_{10}S_2$	721.05	Brown (80)	49.93 (49.97)	3.63 (3.64)	7.76 (7.78)	8.89 (8.91)	7.61 (7.64)
4BNPM $Mn(4BNP)_2(OA_C)_2(H_2O)_2].2H_2O$	$C_{34}H_{34}Mn\ N_4O_{14}S_2$	841.09	Orange (79)	48.52 (48.51)	4.07 (4.10)	6.66 (6.67)	7.62 (7.66)	6.53 (6.56)

Table S4. The molar conductivity and magnetic moment values of the Ni(II) complexes.

Complex	Molar Conductance ($Ohm^{-1}cm^2mol^{-1}$)	μ_{eff} (B.M.)
BAN $[Ni(BA)_2(H_2O)_2].H_2O$	14.7	2.94
BMPN $[Ni(BMP)_2].H_2O$	11.4	3.68
BNPN $[Ni(BNP)_2(H_2O)_2].2H_2O$	13.6	2.92
4BNPN $[Ni(4BNP)_2(OA_C)_2(H_2O)_2].2H_2O$	12.2	2.98

Table S5. The molar conductivity and magnetic moment values of the Mn(II) complexes.

Complex	Molar Conductance ($Ohm^{-1}cm^2mol^{-1}$)	μ_{eff} (B.M.)
BAM $[Mn\ (BA)_2(H_2O)_2].2H_2O$	2.22	5.81
BMPM $[Mn(BMP)_2(H_2O)_2].3H_2O$	3.33	5.95
BNPM $[Mn(BNP)_2(H_2O)_2].2H_2O$	8.55	5.62
4BNPM $[Mn(4BNP)_2(OA_C)_2(H_2O)_2].2H_2O$	12.66	5.32

Table S6. The spectral assignments recorded for the Ni(II) complexes from the UV-Visible spectrum.

Metal complex	UV-Vis Spectral Bands: nm (cm^{-1})	Log ε ($L\ mol^{-1}cm^{-1}$)	Assignment of the Spectral Bands
BAN	287 (34840)	2.80	Intra ligand transition
$[Ni(BA)_2(H_2O)_2].H_2O$	413 (24210)	2.94	Intra ligand transition
	436 (22930)	2.96	Intra ligand transition
	468 (21360)	2.42	CT
	546 (18310)	1.69	$^3A_{2g}(F)\rightarrow{}^3T_{1g}(p)$
BMPN	298 (33550)	2.84	Intra ligand transition
$[Ni(BMP)_2].H_2O$	339 (29490)	2.59	Intra ligand transition
	355(28160)	2.45	Intra ligand transition
	479(20870)	1.83	CT
	556(17980)	1.52	$^3A_{2g}(F)\rightarrow{}^3T_{1g}(p)$
BNPN	305 (32780)	2.94	Intra ligand transition
$[Ni(BNP)_2(H_2O)_2].2H_2O$	376 (26590)	2.64	Intra ligand transition
	418 (23920)	2.79	Intra ligand transition
	454 (22020)	2.93	CT
	554(18050)	0.72	$^3A_{2g}(F)\rightarrow{}^3T_{1g}(p)$
4BNPN	303(33000)	2.88	Intra ligand transition
$[Ni(4BNP)_2(OA_C)_2(H_2O)_2].2H_2O$	341(29320)	2.89	Intra ligand transition
	421(23750)	2.87	Intra ligand transition
	497(20120)	2.56	CT
	565(17690)	1.45	$^3A_{2g}(F)\rightarrow{}^3T_{1g}(p)$

Table S7. The spectral assignments were recorded for the Mn(II) complexes from the UV-Visible spectrum.

Metal Complex	UV-Vis Spectral Bands: nm (cm^{-1})	log ε ($L\ mol^{-1}cm^{-1}$)	Assignments of the Spectral Bands
BAM	267 (37450)	2.27	$\pi\rightarrow\pi^*$
$[Mn\ (BA)_2(H_2O)_2].2H_2O$	314 (31840)	2.84	$n\rightarrow\pi^*$
	347 (28810)	2.68	$n\rightarrow\pi^*$
	431 (23200)	1.74	$^4T_{2g}\leftarrow{}^6A_{1g}$
BMPM	298 (33550)	2.98	$\pi\rightarrow\pi^*$
$[Mn(BMP)_2(H_2O)_2].3H_2O$	335 (29850)	2.80	$n\rightarrow\pi^*$
	351(28490)	2.61	$n\rightarrow\pi^*$
	453 (22070)	1.31	$^4T_{2g}\leftarrow{}^6A_{1g}$
BNPM	270 (37030)	2.35	$\pi\rightarrow\pi^*$
$[Mn(BNP)_2(H_2O)_2].2H_2O$	306 (32670)	2.64	$n\rightarrow\pi^*$
	414 (24150)	2.55	$^4T_{2g}\leftarrow{}^6A_{1g}$
	459 (21780)	2.78	$^4T_{2g}\leftarrow{}^6A_{1g}$

4BNPM	292 (34240)	2.90	$\pi \rightarrow \pi^*$
$[Mn(4BNP)_2(OA_C)_2(H_2O)_2].2H_2O$	344 (29060)	2.66	$n \rightarrow \pi^*$
	409 (24440)	2.98	$^4T_{2g} \leftarrow\!\!- {}^6A_{1g}$
	476 (21000)	2.73	$^4T_{2g} \leftarrow\!\!- {}^6A_{1g}$

Table S8. The characteristic stretching vibrational bands (cm^{-1}) observed for the Ni(II) complexes.

Compound	$\nu_{(OH)}$	$\nu_{(C=N)}$	$\nu_{(C-O)}$	$\nu_{(OAc)}$
BA	3424	1598	1294	-
BAN $[Ni(BA)_2(H_2O)_2].H_2O$	3445	1578	1203	-
BMP	3362	1599	1237	-
BMPN $[Ni(BMP)_2].H_2O$	3384	1539	1222	-
BNP	3354	1590	1274	-
BNPN $[Ni(BNP)_2(H_2O)_2].2H_2O$	3460	1506	1144	-
4BNP	3422	1619	1236	-
4BNPN $[Ni(4BNP)_2(OA_C)_2(H_2O)_2].2H_2O$	3452	1575	1234	ν_{as} 1420, ν_s 1323

Table S9. The characteristic stretching vibrational bands (cm^{-1}) observed for the Mn(II) complexes.

Compound	$\nu_{(OH)}$	$\nu_{(C=N)}$	$\nu_{(C-O)}$	$\nu_{(OAc)}$
BA	3424	1598	1294	-
BAM $[Mn\ (BA)_2(H_2O)_2].2H_2O$	3475	1547	1171	-
BMP	3362	1599	1237	-
BMPM $[Mn(BMP)_2(H_2O)_2].3H_2O$	3414	1547	1259	
BNP	3354	1590	1274	-
BNPM $[Mn(BNP)_2(H_2O)_2].2H_2O$	3371	1555	1201	-
4BNP	3422	1619	1236	-
4BNPM $[Mn(4BNP)_2(OA_C)_2(H_2O)_2].2H_2O$	3457	1577	1236	ν_{as} 1422, ν_s 1326

Table S10. The TG-DTG data recorded for the Ni(II) complexes derived from the Schiff base ligands BA, BMP, BNP and 4BNP.

Complexes	Decomposition Temperature (°C)	DTG Max (°C)	Estimated Weight Loss (%) Calc (Found)	Decomposition of Product Assignments
BAN	166-254	216	8.43 (7.33)	Loss of coordinated water
$[Ni(BA)_2(H_2O)_2].H_2O$	270-332	316	31.47(31.92)	Organic moiety
	484-512	500	17.58 (16.44)	Organic moiety
	538-576	561	20.46 (18.59)	Bulky ligand
BMPN $[Ni(BMP)_2].H_2O$	305-376	341	64.88 (64.28)	Organic moiety
BNPN	207-241	225	8.36 (7.94)	Loss of coordinated water
$[Ni(BNP)_2(H_2O)_2].2H_2O$	314-353	325	63.64 (64.72)	Organic moiety
4BNPN	193-258	227	7.32 (6.99)	Loss of coordinated water
$[Ni(4BNP)_2(OA_C)_2(H_2O)_2].2H_2O$	270-390	318	24.82 (25.33)	Loss of acetate moiety
	423-470	441	19.33 (20.42)	Organic moiety

Table S11. The TG-DTG data recorded for the Mn(II) complexes derived from the Schiff base ligands BA, BMP, BNP and 4BNP.

Complexes	Decomposition Temperature (°C)	DTG max (°C)	Estimated Weight Loss (%) Calc (Found)	Decomposition of Product Assignments
BAM	160-237	180	7.05 (6.97)	Loss of coordinated water
$[Mn\ (BA)_2\ (H_2O)_2].2H_2O$	198-374	317	34.8 (35.53)	Organic moiety (ligand)
	436-580	497	10.66 (11.23)	Organic moiety
BMPM	122-207	178	5.47 (5.61)	Loss of coordinated water
$[Mn(BMP)_2(H_2O)_2].3H_2O$	252-375	317	60.60 (59.42)	Organic moiety (ligand)
	444-565	498	19.86 (18.55)	Organic moiety (ligand)
BNPM	191-247	238	7.76 (7.09)	Loss of coordinated water
$[Mn(BNP)_2(H_2O)_2].2H_2O$	255-360	289	24.54 (25.94)	Organic moiety (ligand)
	466-570	504	25.36 (26.19)	Organic moiety (ligand)
4BNPM	171-267	220	8.66 (7.86)	Loss of coordinated water
$[Mn(4BNP)_2(OA_C)_2(H_2O)_2].2H_2O$	268-290	280	17.28 (18.33)	Loss of acetate moiety
	288-380	313	22.17 (23.05)	Organic moiety (ligand)
	419-516	464	28.45 (27.37)	Organic moiety (ligand)

Table S12. The values of the minimal inhibitory concentration of the chosen compound against bacterial and fungi strains.

Compounds	**MIC values (µg/mL)**			
	E. coli	***P. aeruginosa***	***B. subtilis***	***S. aureus***
BAM	63.4	56.7	51.4	63.7
BMPN	59.6	49.5	54.3	41.9
BNPN	57.3	47.4	31.4	38.8
Ciprofloxacin	>7	0	>7	>7

Table S13. The percentage of the inhibition and the IC_{50} values of the synthesized Schiff base ligands and their transition metal complexes.

Compound	IC_{50} (mM) α-amylase
Acarbose	0.033 ±0.008
BA	0.043 ± 0.100
BAN	-
BAM	-
BMP	0.047 ± 0.100
BMPN	0.139 ± 0.300
BMPM	0.108 ± 0.300
BNP	-
BNPN	-
BNPM	0.056 ± 0.200
4BNP	-
4BNPN	0.053 ± 0.200
4BNPM	-

Table S14. The modulation of the α-amylase activity, impact on K_m, V_m and K_i, inhibition mode on the Schiff base ligand BA and their Ni(II), and Mn(II) complexes.

Compound	K_m (mM)	V_m (µmol/min)	K_i (mM)	Mode of Inhibition
Control	0.580	1.256		
BA	0.580	0.628	0.468	Non-Comp
Control	0.650	1.152		
BAN	0.650	0.576	0.788	Non-Comp
Control	0.800	1.216		
BAM	0.800	0.608	0.433	Non-Comp
Control	0.580	1.156		
BMP	0.580	0.578	0.457	Non-Comp
Control	0.749	1.270		
BMPN	0.749	0.635	0.526	Non-Comp
Control	1.316	1.404		
BMPM	1.316	0.702	0.423	Non-Comp
Control	0.580	1.168		
BNP	0.580	0.584	0.521	Non-Comp
Control	1.547	1.348		
BNPN	1.547	0.674	0.378	Non-Comp
Control	1.923	1.464		
BNPM	1.923	0.732	0.457	Non-Comp
Control	0.580	1.382		
4BNP	0.580	0.691	0.414	Non-Comp
Control	0.748	1.344		
4BNPN	0.748	0.672	0.545	Non-Comp
Control	1.031	1.617		
4BNPM	1.031	0.808	0.426	Non-Comp

Table S15. The global descriptors of the Schiff base ligands including the chemical potential, chemical hardness, chemical softness, electronegativity nucleophilicity, and electrophilicity are calculated using **Equations S1 to S6.**

The theorem developed by Koopman's, 'I' denotes the ionization potential obtained from -$E_{HOMO,}$ and 'A' is the electron affinity equal to $-E_{LUMO}$.

$$\text{Electronegativity } (\chi) = \frac{I + A}{2} \qquad \text{Eqn. (S1)}$$

$$\text{Chemical hardness } (\eta) = \frac{I - A}{2} \qquad \text{Eqn. (S2)}$$

$$\text{Chemical potential } (\mu) = -\chi \qquad \text{Eqn. (S3)}$$

$$\text{Chemical softness (S)} = \frac{1}{2\eta} \qquad \text{Eqn. (S4)}$$

$$\text{Electrophilicity index } (\omega) = \frac{\mu\text{^}2}{2\eta} \qquad \text{Eqn. (S5)}$$

$$\text{Nucleophilicity index (n)} = 1/\omega \qquad \text{Eqn. (S6)}$$

Table S16. The calculated theoretical quantum chemical parameters for the synthesized Schiff base ligands.

Compounds	**-E_{HOMO} (eV)**	**-E_{LUMO} (eV)**	**ΔE (eV)**	**χ (eV)**	**Ƞ (eV)**	**(μ) (eV)**	**S (eV)**	**ω (eV)**	**n (eV)**
BA	-5.88	-2.17	3.71	4.02	1.85	-4.02	0.26	4.37	0.22
BMP	-5.79	-2.13	3.65	3.96	1.82	-3.96	0.27	4.30	0.23
BNP	-6.34	-2.68	3.66	4.51	1.83	-4.51	0.27	5.55	0.18
4BNP	-6.26	-2.61	3.65	4.43	1.82	-4.43	0.27	5.38	0.18

Table S17. The calculated theoretical quantum chemical parameters for the metal complex BAN derived from the Schiff base ligand BA.

BAN	**eV**
HOMO	-5.66
LUMO	-2.64
Energy Gap ΔE	3.02
Ionization Energy (I = ε HOMO = -HOMO)	5.66
Electron Affinity (A= ε LUMO = -LUMO)	2.64
Global Hardness (η = (I-A)/2)	1.51
Global Softness (S = 1/η)	0.66
Chemical Potential (μ =- (I+A)/2)	-4.15
Electronegativity (χ = -μ)	4.15
Electrophilicity index (ω = μ2/2η	5.70
Nucleophilicity index (N = 1/ω)	0.18
ΔN max	2.74
Electron accepting power ω+= A2/2(I-A)	1.15
Electron donating power ω+= I2/2(I-A)	14.24

Table S18. The calculated theoretical quantum chemical parameters for the metal complex BAM derived from the Schiff base ligand BA.

BAM	**eV**
HOMO	-2.28
LUMO	-0.42
Energy Gap ΔE	1.86
Ionization Energy (I = ε HOMO = -HOMO)	2.28
Electron Affinity (A= ε LUMO = -LUMO)	0.42
Global Hardness (η = (I-A)/2)	0.93
Global Softness (S = 1/η)	1.07
Chemical Potential (μ =- (I+A)/2)	-1.35
Electronegativity (χ = -μ)	1.35
Electrophilicity index (ω = μ2/2η	0.98
Nucleophilicity index (N = 1/ω)	1.02
ΔN max	1.45
Electron accepting power ω+= A2/2(I-A)	0.05
Electron donating power ω+= I2/2(I-A)	-5.13

Table S19. The calculated theoretical quantum chemical parameters for the metal complex BMPN derived from the Schiff base ligand BMP

BMPN	**eV**
HOMO	-5.13
LUMO	-2.55
Energy Gap ΔE	2.58
Ionization Energy (I = ε HOMO = -HOMO)	5.13
Electron Affinity (A= ε LUMO = -LUMO)	2.55
Global Hardness (η = (I-A)/2)	1.29
Global Softness (S = 1/η)	0.78
Chemical Potential (μ =- (I+A)/2)	-3.84
Electronegativity (χ = -μ)	3.84
Electrophilicity index (ω = μ2/2η	5.73
Nucleophilicity index (N = 1/ω)	0.17
ΔN max	2.98
Electron accepting power ω+= A2/2(I-A)	1.27
Electron donating power ω+= I2/2(I-A)	10.40

Table S20. The calculated theoretical quantum chemical parameters for the metal complex BMPM derived from the Schiff base ligand BMP.

BMPM	**eV**
HOMO	-3.52
LUMO	-0.88
Energy Gap ΔE	2.64
Ionization Energy (I = ε HOMO = -HOMO)	3.52
Electron Affinity (A= ε LUMO = -LUMO)	0.88
Global Hardness (η = (I-A)/2)	1.32
Global Softness (S = 1/η)	0.76
Chemical Potential (μ =- (I+A)/2)	-2.20
Electronegativity (χ = -μ)	2.20
Electrophilicity index (ω = μ2/2η	1.84
Nucleophilicity index (N = 1/ω)	0.54
ΔN max	1.67
Electron accepting power ω+= A2/2(I-A)	0.15
Electron donating power ω+= I2/2(I-A)	-14.21

Table S21. The calculated theoretical quantum chemical parameters for the metal complex BNPN derived from the Schiff base ligand BNP.

BNPN	**eV**
HOMO	-5.77
LUMO	-3.02
Energy Gap ΔE	2.75
Ionization Energy (I = ε HOMO = -HOMO)	5.77
Electron Affinity (A= ε LUMO = -LUMO)	3.02
Global Hardness (η = (I-A)/2)	1.38
Global Softness (S = 1/η)	0.73
Chemical Potential (μ =- (I+A)/2)	-4.39
Electronegativity (χ = -μ)	4.39
Electrophilicity index (ω = μ2/2η	7.01
Nucleophilicity index (N = 1/ω)	0.14
ΔN max	3.19
Electron accepting power ω+= A2/2(I-A)	1.65
Electron donating power ω+= I2/2(I-A)	10.15

Table S22. The calculated theoretical quantum chemical parameters for the metal complex BNPM derived from the Schiff base ligand BNP.

BNPM	**eV**
HOMO	-2.95
LUMO	-0.44
Energy Gap ΔE	2.51
Ionization Energy (I = ε HOMO = -HOMO)	2.95
Electron Affinity (A= ε LUMO = -LUMO)	0.44
Global Hardness (η = (I-A)/2)	1.25
Global Softness (S = 1/η)	0.80
Chemical Potential (μ =- (I+A)/2)	-1.69
Electronegativity (χ = -μ)	1.69
Electrophilicity index (ω = μ2/2η	1.14
Nucleophilicity index (N = 1/ω)	0.88
ΔN max	1.35
Electron accepting power ω+= A2/2(I-A)	0.04
Electron donating power ω+= I2/2(I-A)	-5.31

Table S23. The calculated theoretical quantum chemical parameters for the metal complex 4BNPN derived from the Schiff base ligand 4BNP.

4BNPN	**eV**
HOMO	-6.14
LUMO	-3.10
Energy Gap ΔE	3.05
Ionization Energy (I = ε HOMO = -HOMO)	6.14
Electron Affinity (A= ε LUMO = -LUMO)	3.10
Global Hardness (η = (I-A)/2)	1.52
Global Softness (S = 1/η)	0.66
Chemical Potential (μ =- (I+A)/2)	-4.62
Electronegativity (χ = -μ)	4.62
Electrophilicity index (ω = μ2/2η	7.01
Nucleophilicity index (N = 1/ω)	0.14
ΔNmax	3.04
Electroaccepting power ω+= A2/2(I-A)	1.58
Electrodonating power ω+= I2/2(I-A)	11.97

Table S24. The calculated theoretical quantum chemical parameters for the metal complex 4BNPM derived from the Schiff base ligand 4BNP.

4BNPM	**eV**
HOMO	-2.58
LUMO	0.13
Energy Gap ΔE	2.70
Ionization Energy (I = ε HOMO = -HOMO)	2.58
Electron Affinity (A= ε LUMO = -LUMO)	-0.13
Global Hardness (η = (I-A)/2)	1.35
Global Softness (S = 1/η)	0.74
Chemical Potential (μ =- (I+A)/2)	-1.22
Electronegativity (χ = -μ)	1.22
Electrophilicity index (ω = μ2/2η	0.55
Nucleophilicity index (N = 1/ω)	1.80
ΔN max	0.91
Electron accepting power ω+= A2/2(I-A)	0.00
Electron donating power ω+= I2/2(I-A)	-2.24